

**SPATIALLY FRACTIONATED PROTON THERAPY: A MONTE CARLO
VERIFICATION**

A Thesis
Presented to
The Academic Faculty

By

Jenna Fair

In Partial Fulfillment
Of the Requirements for the Degree
Master of Science in Medical Physics

Georgia Institute of Technology

May 2016

Copyright © Jenna Fair 2016

**SPATIALLY FRACTIONATED PROTON THERAPY: A MONTE CARLO
VERIFICATION**

Approved by:

C-K Chris Wang, PhD
Woodruff School of Mechanical Engineering
Georgia Institute of Technology

Lei Zhu, PhD
Woodruff School of Mechanical Engineering
Georgia Institute of Technology

Eric Elder, PhD
Medical Physicist
Emory University Hospital

Date Approved: 22 April 2016

ACKNOWLEDGEMENTS

I would like to thank my brother, mother, and father for their unwavering support during my time at Georgia Tech. I would also like to thank Dr. Chris Wang for his knowledge, help, and guidance. Additionally, I would like to thank Jackson Renegar for his contribution of clinical knowledge to the project.

TABLE OF CONTENTS

	Page
ACKNOWLEDGEMENTS	iii
LIST OF TABLES	vi
LIST OF FIGURES	vii
LIST OF SYMBOLS AND ABBREVIATIONS	ix
SUMMARY	x
CHAPTER 1: INTRODUCTION	1
CHAPTER 2: MOTIVATION & OBJECTIVE	5
CHAPTER 3: OVERVIEW OF PROTON THERAPY	7
3.1 Proton Overview	7
3.1.1 Proton Interactions	7
3.1.2 Proton Radiobiology	9
3.2 Proton Facility Overview	10
3.2.1 Proton Facility Design	10
3.2.2 Cyclotron Operation	11
3.2.3 Pencil Beam Scanning	13
3.3 X-Ray grid Therapy Overview	14
3.3.1 X-Ray grid Therapy Design	14
3.3.2 Radiobiology of X-Ray grid Therapy	16
3.4 Application of grid Therapy to Protons	17
CHAPTER 4: MCNP6 MODEL OF CLINICAL PROTON BEAM	19
4.1 Macroscopic Geometry in MCNP6	19
4.2 Proton Beam Geometry in MCNP6	21
4.3 Dose Calculation in MCNP6	25
4.4 Dose Calculation in RayStation	27
4.5 Experimental Setup and Dose Measurement Using Gafchromic EBT3 Film	28
CHAPTER 5: MCNP6, RAYSTATION, AND EXPERIMENTAL RESULTS	30
5.1 MCNP6 Results	30
5.1.1 Percentage Depth Dose	30
5.1.2 Gaussian Beam Profile	31
5.1.3 Spatially Fractionated Proton Dose Distributions	33
5.2 Comparison of MCNP6 and RayStation Results	37

5.3 Comparison of MCNP6 and Gafchromic Film Results	40
5.4 Comparison of Spatially Fractionated Proton Therapy to Photon Grid Therapy	44
CHAPTER 6: CONCLUSIONS AND FUTURE WORK.....	46
6.1 Conclusions.....	46
6.2 Future Work.....	47
APPENDIX A: MCNP INPUTS	49
A.1 MCNP6 PDD Input.....	49
A.2 MCNP6 Beam 11 TMESH1 Tally Input at the Surface.....	67
A.3 MCNP6 Beam 11 TMESH3 Tally Input at the Surface.....	68
APPENDIX B: MATLAB ANALYSIS FILES.....	69
B.1 TMESH Tally Code: MdataReader.....	69
B.2 TMESH Tally Code: ReadMData	69
B.3 TMESH Tally Code: ReadFortranBinary	72
B.4 TMESH Tally Code: NextRecord	73
B.5 TMESH Tally Code: ReadRecord.....	74
B.6 Gamma Analysis Code: CalcGamma.....	74
REFERENCES	88

LIST OF TABLES

	Page
Table 4.1: 121 MeV FWHM Data	20
Table 4.2: SI1, SP1, and SB1 Values for 121 MeV Proton Beam at Isocenter	23
Table 4.3: Unit Vectors for 121 MeV Proton Beam.....	24
Table 5.1: Corner Beamlet Locations	35
Table 5.2: MCNP6 Radial and Transverse PVDR's.....	36
Table 5.3: RayStation Radial and Transverse PVDR's	38

LIST OF FIGURES

	Page
Figure 1.1: Proton Dose Deposition as a Function of Depth	1
Figure 1.2: Spread-Out Bragg Peak	2
Figure 1.3: Collimator Used for Grid Therapy	3
Figure 3.1: Collision Parameters for a Charged Particle	8
Figure 3.2: Depth-Dose Curve of High and Low Energy Protons.....	9
Figure 3.3: Blueprint of Provision Proton Therapy, Knoxville, Tennessee	11
Figure 3.4: Cyclotron Components.....	12
Figure 3.5: Range Modulation Wheel.....	13
Figure 3.6: Varian Grid Block	15
Figure 3.7: Schematic of Grid Collimator at Isocenter.....	16
Figure 4.1: MCNP6 Macroscopic Geometry (Not Drawn to Scale).....	19
Figure 4.2: Hexagonally Packed Array of 121 MeV Proton Beams at Isocenter	21
Figure 4.3: CAX Beam Source Card	22
Figure 4.4: Point Source Collimated into Cone of Directions	22
Figure 4.5: TMESH1 Tally Card	25
Figure 4.6: Experimental Setup of Solid Water and Gafchromic EBT3 Films	28
Figure 5.1: Percentage Depth Dose for 121 MeV Protons	31
Figure 5.2: Transverse Profile of CAX Beam at Surface of Water Phantom	32
Figure 5.3: Dose Distribution of the CAX Beam at the Surface of the Water Phantom	32
Figure 5.4: MCNP6 Dose Distribution at (a) Surface, (b) 5 cm, (c) 10.8 cm.....	34

Figure 5.5: MCNP6 (a) Transverse and (b) Radial Dose Profiles	36
Figure 5.6: MCNP6 and RayStation Transverse Profiles	37
Figure 5.7: Gamma Analysis between MCNP6 and Raystation.....	39
Figure 5.8: Gafchromic EBT3 Films Post-Irradiation	40
Figure 5.9: Gafchromic Film Dose Distribution at 10.8 cm Post-Processing	41
Figure 5.10: Gafchromic Film at 10.8 cm Before and After Processing	42
Figure 5.11: MCNP6 and Gafchromic Film Transverse Profiles	43
Figure 5.12: Gamma Analysis between MCNP6 and Gafchromic Film	44

LIST OF SYMBOLS AND ABBREVIATIONS

SOBP.....	Spread-out Bragg peak
SFPT	Spatially fractionated proton therapy
eV	Electron volts
LET	Linear energy transfer
AC	Alternating current
PBS	Pencil beam scanning
Energy selection system.....	ESS
FWHM	Full-width half-maximum
c-t-c	Center-to-center
RIBE	Radiation induced bystander effect
TR	Therapeutic ratio
SSD	Source-to-surface distance
CAX	Central axis
Gy.....	Gray
PVDR.....	Peak-to-valley dose ratio
DTA	Distance-to-agreement

SUMMARY

Spatially fractionated radiation therapy (or grid) using megavoltage x-rays is a relatively new method of treating bulky (>8 cm) malignant tumors. Unlike the conventional approach in which the entire tumor is targeted with a nearly uniform radiation field, in grid the incident radiation is collimated with a special grid collimator. As such, only the volume under the open areas of the grid receives direct irradiation from the incident beam; the rest only sees scattered radiation and hence receives significantly less dose. Those regions seeing less dose serve as regrowth areas for normal tissues, thus reducing the normal tissue complication probability after the treatment. Although the grid dose distribution in a tumor is non-uniform, the regression of tumor mass has exhibited uniform regression clinically. One plausible explanation might be the enhanced re-oxygenation of the tumor following grid.

Protons have two advantages over megavoltage x-rays which are typically used for grid: (1) protons scatter less in tissue, and (2) they have a fixed range in tissue (the Bragg peak) that can be used to target a tumor. The goal of this thesis is to computationally and experimentally assess the feasibility of grid using clinical proton beams. The proton pencil beams at the Provision Cancer Center in Knoxville, Tennessee, are used to create an array of beams mimicking the arrangement of beams in grid therapy. The dose distributions at various depths in a solid-water phantom are obtained computationally by the Monte Carlo code MCNP and experimentally by Gafchromic film EBT3. The results will be compared with those of the grid using megavoltage x-rays.

CHAPTER 1: INTRODUCTION

Upon the advent of the cyclotron in the early twentieth century, Robert R. Wilson discovered the potential for the therapeutic use of protons in 1946. At the time, therapeutic treatments were limited to using photons and electrons due to the low penetration of moderate energy protons. Using a cyclotron, protons and other particles could be accelerated to high speeds and consequently high energies making them an ideal candidate for treating deep-seated tumors.

Additionally, the depth-dose profile of the proton makes it therapeutically ideal. As shown in Figure 1.1, the proton deposits a majority of its dose at the location of the Bragg peak. The depth of the Bragg peak is a function of the energy of the proton: as the energy of the incident proton increases, so does the depth of the Bragg peak. The average entrance dose delivered to normal tissue by the incident proton is also much lower, and there is no exit dose. The combination of these three characteristics allows for better delivery of dose to the target volume as well as decreased dose to healthy surface tissue and healthy tissue beyond the target volume.

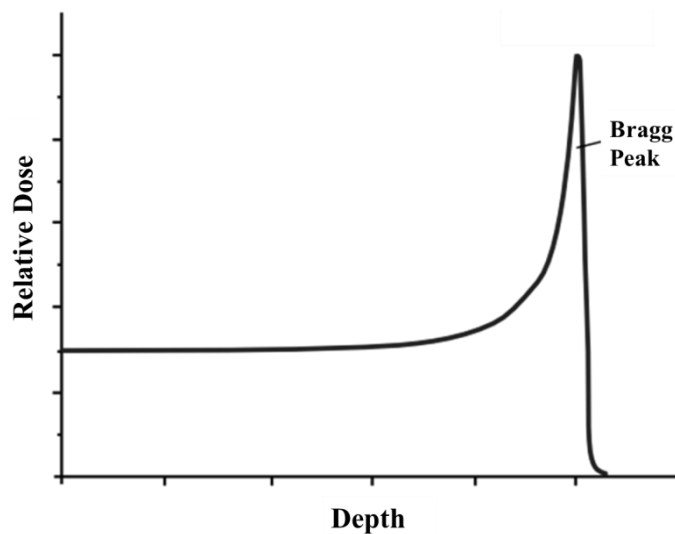


Figure 1.1: Proton Dose Deposition as a Function of Depth [1]

A target volume such as a tumor has three dimensions: its size in the lateral direction (x- and y-directions) and its depth or thickness (z-direction). To create homogenous dose in the lateral direction, pencil beam scanning is performed in which the proton beam is scanned in the x- and y-directions over the lateral area of the target. To create dose throughout the depth of the target volume (z-direction), varying energies are used to create a spread-out Bragg peak (SOBP), shown in Figure 1.2. The dotted line represents a single Bragg peak from the highest energy proton used to create the SOBP. By also delivering dose using subsequently lower energies, multiple Bragg peaks occur at shallower depths. Upon summation of the dose deposition from the multiple proton beams, the SOBP is calculated and is shown as the solid line. Using the SOBP method, the tumor receives 100% of the prescribed dose while minimizing dose to surface tissue and eliminating exit dose. This is in stark contrast to the dose distribution due to traditional megavoltage x-ray treatment which is shown by the dashed line. To achieve 100% of the prescription dose in the tumor volume, there is undesired dose delivered to healthy surface and exit tissues when photon radiation therapy is used.

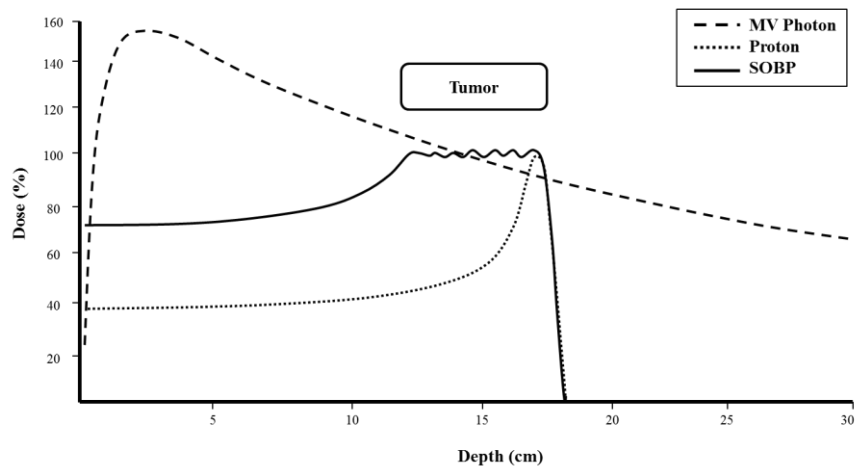


Figure 1.2: Spread-Out Bragg Peak

In spatially fractionated megavoltage x-ray (grid) therapy, a special collimator is used to collimate the x-ray into multiple circular beams in a grid-like array, shown in Figure 1.3. The collimator is typically made of brass or Cerrobend, and the divergence of the holes matches the divergence of the x-ray beam from the linear accelerator.



Figure 1.3: Collimator Used for Grid Therapy [2]

Grid therapy makes use of the bystander effect by delivering a high dose in a single fraction to exposed regions and delivering only scatter dose to those regions blocked by the collimator. The underdosed regions serve as areas for the regrowth of normal tissue. It has been proven that the use of high-dose, single fraction grid therapy is advantageous for tumor cell killing and healthy cell sparing if the tumor cells are equally or more radioresistant than the healthy tissue cells [3].

This is in contrast to the traditional belief that a tumor should receive uniform dose. The bystander effect describes a series of radiation signaling events that results in programmed cell death (apoptosis) from the release of cytokines from neighboring cells. Additionally, tumor cells

are less radioresistant when oxygenated. Upon grid irradiation, some of the tumor volume is killed resulting in redirected blood flow to and oxygenation of the surviving tumor cells. Grid therapy makes use of both of these principles. Although the grid dose distribution is non-uniform, observed tumor regression is clinically uniform [4].

Spatially fractionated proton therapy (SFPT) has yet to be investigated, but there is promise that a similar dose distribution can be manufactured using clinical proton beams. Because of the small circular shape of the beam at the surface of the patient, there is no manufactured collimator needed for treatment. Additionally, protons have two advantages over x-rays: they scatter less in tissue, and they deposit most of their dose at the predetermined Bragg peak delivering significantly less dose to entrance and exit regions. Chapter 2 focuses on the motivation for and the objective of modeling SFPT in MCNP6. Chapter 3 provides a background of the general physics associated with proton therapy as well as the radiobiological principles at play in grid radiotherapy. Chapter 4 discusses the setup and beam parameters used to run the MCNP6 simulations, the treatment planning system validation, and the experimental film validation as well as the methods used for dose calculation. Chapter 5 presents the results of MCNP6 simulations and validates the model using the treatment planning system and experimental film data. A comparison between SFPT and traditional grid therapy is also presented in this chapter. Chapter 6 concludes this project's work and offers suggestions for future research based on this thesis.

CHAPTER 2: MOTIVATION & OBJECTIVE

Due to the increased cost of proton therapy, there must be a marked dosimetric advantage observed in order to warrant its clinical use in lieu of x-ray grid therapy. It has already been exhibited that x-ray grid therapy produces clinically favorable results due to an increased therapeutic ratio. In particular, it is advantageous to use grid therapy prior to traditional therapies that may not be successful in cases where the normal tissue is radiosensitive, the tumor is acutely responding, and the tumor is bulky ($> 8\text{cm}$) [5]. These assertions were validated by a dosimetric MCNP6 study in which the x-ray beam and grid block were included in the simulations. In most cases, grid therapy is used as a supplement to traditional x-ray therapy in order to de-bulk a large tumor.

The motivation behind using protons stems from a desire to increase local control and decrease normal tissue complication probability. The basic physics of the proton's dose deposition associated with its high energy indicates that the dose can be better targeted to the tumor while delivering significantly less dose to healthy entrance and exit tissues. This decreases normal tissue complication probabilities which are often seen as adverse side effects, a direct result of overdosing healthy functional tissues in order to maximize the dose to the tumor.

In order to observe dose deposition due to protons, software that can model complex geometries and primary and secondary interactions is necessary. MCNP6 is an ideal software to use since it is a Monte Carlo simulation program that allows the user to create the geometry, the source, and the lattice structure used to model and calculate the complex dose deposition. The objective of this study is to model SFPT in MCNP6 and to compare the results with those of the experimental films and the treatment planning system. MCNP6 has the capabilities to model

proton dose delivery unlike its predecessors. Using this software, the dose distribution of a spatial array of proton beams can be observed. While MCNP6 is an ideal software to use for this research, it can be difficult and cumbersome to use in a clinical setting due to the extensive amount of modeling parameters needed to satisfy requirements. Additionally, the computational time required to run Monte Carlo calculations is significant; however, in traditional treatment planning systems, there are now Monte Carlo dose calculation algorithms available for physicists and dosimetrists to use. These methods model reality very well.

The focus of this work is to evaluate the effectiveness of using MCNP6 to model SFPT as well as to match the spatial dose distribution of proton therapy to that of x-ray grid therapy. To evaluate the effectiveness of the MCNP6 model, the results of MCNP6 are compared with the results obtained from the treatment planning system and experimental data collected from Provision Therapy Center in Knoxville, Tennessee.

CHAPTER 3: Overview of Proton Therapy and Grid Therapy

The goal of proton therapy, like all radiation therapy techniques, is to accurately deliver dose to unhealthy tissue while sparing healthy tissue. In order to do so, the physics behind the production of therapeutic protons must be well understood. In this section, the basic physics of proton therapy and grid therapy are discussed. The physics behind the production of high energy protons as well as the radiobiological aspects of grid therapy are also examined in order to prepare for the discussion of the SFPT model in Chapter 4.

3.1 Proton Overview

3.1.1 Proton Interactions

Like any charged particle, protons interact with other atoms via soft and hard collisions. Figure 3.1 shows the impact parameters a and b . Parameter a is the distance from the center of the nucleus to the edge of the electron cloud, and parameter b is the distance from the center of the nucleus to the trajectory path. Hard collisions occur when a proton interacts with a single atomic electron: parameter b is approximately equal to parameter a . The energy transferred from the proton to the atomic electron is great enough that the electron is ejected from the atom as a delta ray (i.e. an energetic knock-out electron). When parameter b is less than parameter a , the proton undergoes Coulombic interactions with the nucleus. In this case, its direction may change but its energy loss is insignificant.

The most numerous type of collision, however, is the soft collision: parameter b is greater than parameter a . Soft collisions are the primary mechanism responsible for energy deposition by charged particles in a medium. The influence of the proton's force is felt by the entire atom resulting in excitation or ionization of the atom. In each interaction, only a few electron volts

(eV) are deposited, but since these events are so numerous, the aggregate energy deposition is great. In addition to soft and hard collisions, another mechanism by which protons may deposit energy is a nuclear reaction, but this is a rare occurrence and will not be discussed further in this model.

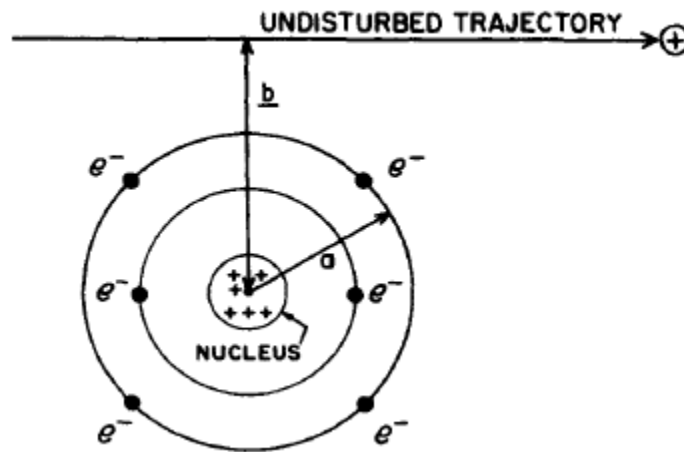


Figure 3.1: Collision Parameters for a Charged Particle [1]

The rate at which a charged particle deposits energy in a medium is described as the stopping power, which is also called, linear energy transfer (LET), and is characterized by the Bethe-Bloch equation [1]. The LET is the amount of energy transferred from a charged particle per unit path length. The LET of a heavy charged particle is inversely proportional to the square of the velocity of the particle; therefore, as the proton loses energy, its LET increases.

Figure 3.2 depicts the Bragg peak, the point at which the proton deposits its energy with its highest LET. As the proton slows down in the medium and loses energy, its LET increases. The increase in LET causes an increase in absorbed dose. As shown, the Bragg peak occurs at a location slightly before where the proton stops. If the energy of the proton is greater, the depth

of the Bragg peak is greater as well. This is because it takes higher energy protons a greater amount of distance to slow down to a stop.

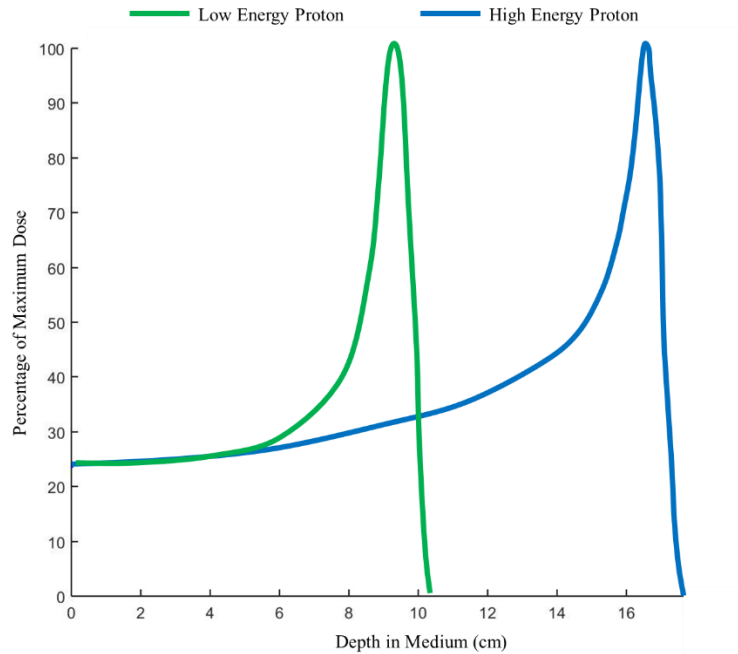


Figure 3.2: Depth-Dose Curve of High and Low Energy Protons

3.1.2 Proton Radiobiology

The most appealing qualities of proton therapy arise from its radiobiological characteristics. The relative biological effectiveness (RBE) is the ratio of the dose of a high energy photon beam to the dose of the reference radiation which produces the same effects, shown in Equation 1.

$$\text{Equation 1: } RBE = \frac{\text{Dose of high energy photon}}{\text{Dose of reference radiation (i.e.proton)}}$$

The RBE of proton therapy relative to photon therapy is around 1.1, and it can range from 1.1 at the entrance region to 1.7 in the distal falloff region [6]. With an RBE greater than one, the amount of dose needed from the proton beam to produce the same biological effect as the high energy photon beam is less, meaning that protons are more effective at cell killing [6].

The difference in the RBE's of protons and high energy photons is the result of dose, dose fractionation, dose rate, and radiation quality. The most relevant cause of RBE difference is radiation quality or LET. Protons, in general, have higher LET than photons, and, as such, they deposit energy more densely along their track. Specifically, the high LET of the protons close to the Bragg peak results in an increased probability of DNA damage per unit path length. An RBE of more than one in conjunction with the defined range of the proton's Bragg peak make it an ideal substitute for high energy photon therapy in some cases.

3.2 Proton Facility Overview

3.2.1 Proton Facility Design

A blueprint of the Provision Proton Therapy Center in Knoxville, Tennessee, is shown in Figure 3.3. Provision is the center that provided the beam data used to construct the model in Chapter 4 as well as the treatment planning system and experimental data used to validate the model in Chapter 5. The center is equipped with two separate systems. The first system is an IBA/Varian system which supplies three treatment rooms with a high energy proton beam, highlighted in green in Figure 3.3. The second system, highlighted in blue in Figure 3.3, is a ProNova system that supplies two treatment rooms with a high energy proton beam. Each system uses its own cyclotron to produce high energy protons which are then transported through a series of bending magnets, altering the path of the proton so that it appropriately enters the treatment room.

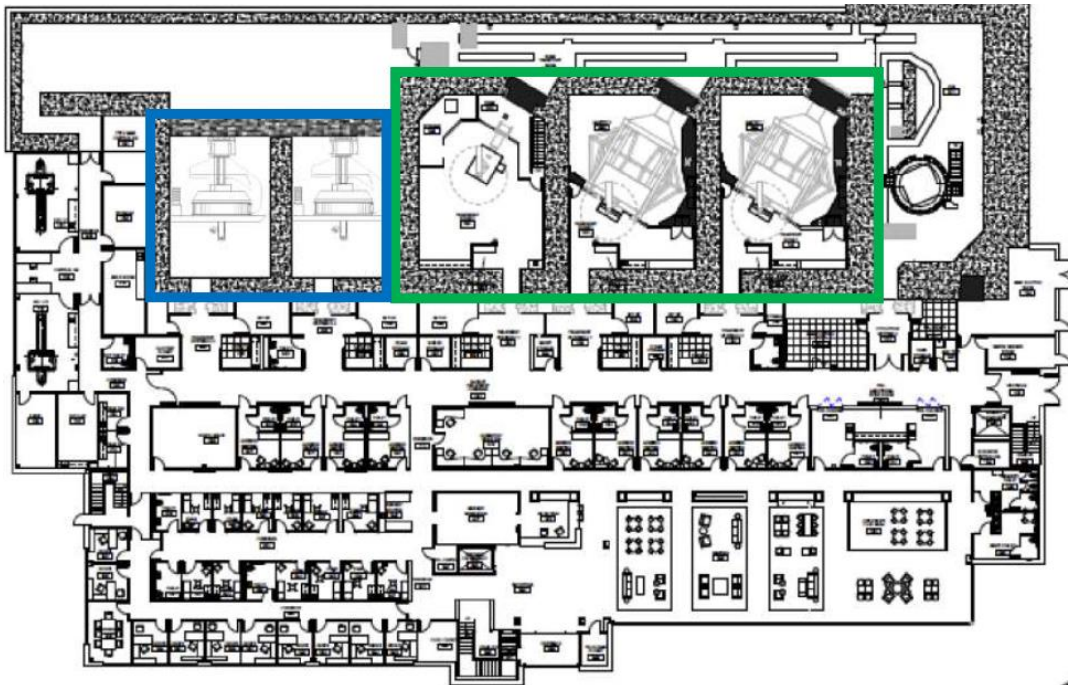


Figure 3.3: Blueprint of Provision Proton Therapy, Knoxville, Tennessee [7]

The new ProNova system provides the ability to achieve 360° rotation around the patient in the treatment room, similarly to conventional x-ray linear accelerators. By using superconducting magnets, the size, weight, and bending radius of the entire system are significantly reduced, in turn decreasing construction and real estate costs. Construction on the ProNova system is currently being completed, so the IBA/Varian pencil beam scanning system will be used to validate the MCNP6 model discussed in Chapter 4.

3.2.2 Cyclotron Operation

The high energy protons that are transported through the bending magnets are first created and accelerated in a cyclotron. A typical cyclotron is shown in Figure 3.4. The cyclotron is comprised of two hollow semicircular metal electric diodes called dees, a name derived from their D-like shape. The two dees are separated by a gap over which an alternating voltage is

applied. The ion source is located in the center of the two dees. Above and below the dees are two magnets which cause the circular trajectory of the charged particles inside the cyclotron.

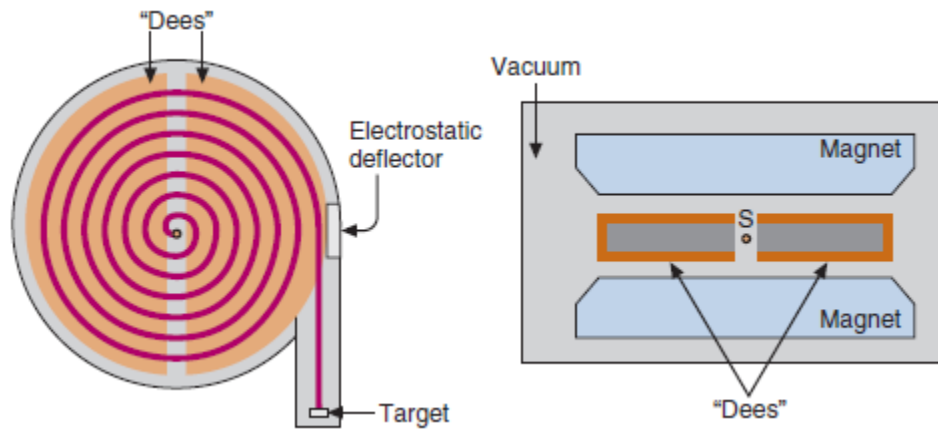


Figure 3.4: Cyclotron Components [8]

The process begins by separating the charged particle from an atom in the ion source located in the center of the dees. The protons are separated in short bursts upon which they are ejected into the gap where they are accelerated by the alternating current (AC) voltage. The protons continue their circular trajectory around the cyclotron because of the magnetic field. Each time the proton passes through the gap in between the dees, it is accelerated by approximately 30 keV. This increase in energy directly compensates for the increased pathlength experienced by the proton in each sequential rotation, so the accelerating AC voltage remains in phase with the time at which the protons pass through the gap. Once the proton reaches its desired energy, it is ejected from the cyclotron.

After ejection from the cyclotron, the proton enters a series of conducting magnets. Since proton accelerator facilities are so expensive, it is common to use one stream of protons from one

cyclotron to supply several rooms with a treatment beam. The magnets redirect the travel path of the proton beam so that it enters each treatment room at the appropriate point and angle.

3.2.3 Pencil Beam Scanning

There are two types of treatment methods used today in proton therapy. The first technique, passive spreading, uses scattering material to create a uniform field [9]. A single scattering layer is used for small fields, and two scattering layers are used for large fields. Additionally, a range modulation wheel is used to create the SOBP. The range modulation wheel in Figure 3.5 achieves different energies from the monoenergetic treatment beam. Each step on the range modulation wheel acts as a specific energy degrader. The thickness of the modulation wheel is inversely proportional to the energy of the proton after degradation: the thicker the step, the lower the energy. A compensator is also needed to shape the proton field to the appropriate tumor geometry.



Figure 3.5 Range Modulation Wheel [10]

The second method in use is active spreading, more commonly known as pencil beam scanning (PBS). PBS uses magnets to deflect and steer the proton beam [9]. In passive

spreading, the machine output is a uniform area of proton beam; however, in active spreading, the machine output is a small pencil-like beam that is used to paint the dose over the tumor area. Unlike passive spreading, PBS does not require the use of scattering materials, so there is less secondary radiation. Additionally, PBS does not require the use of a compensator, negating the need for patient-specific compensator production. The resultant energy in PBS is selected upstream from the treatment room by the energy selection system (ESS). The ESS consists of a set of absorbers, an achromatic dipole, and a set of slits to limit emittance and prevent beam spread [11]. Together, these components create a lower energy monoenergetic proton beam from the high energy beam emitted from the cyclotron. The proton beam size varies as a function of the energy. This effect is caused by Coulombic interactions between the protons in the beam. Since all protons have the same charge, they experience a repulsive force from other protons within the beam. At lower energies, the beam spread effect is more pronounced because of the higher likelihood of interaction due to the lower speed of the particles. As the proton energy is increased, the likelihood of Coulombic interaction decreases because the particles are moving at a higher speed; therefore, as the energy of the proton beam increases, the full-width half-maximum (FWHM) of the beam decreases.

3.3 X-Ray grid Therapy Overview

3.3.1 X-Ray grid Therapy Design

Spatially fractionated x-ray therapy (grid therapy) collimates a broad x-ray field to make use of certain radiobiological properties. A commercially available grid block is shown in Figure 3.6. This is a Varian block made of a low melting alloy. The low melting alloy used is Cerrobend with a thickness of 7.5 cm [5]. The block features divergent collimator holes arranged in a honeycomb fashion. At 100 cm distance from the treatment head of the linear

accelerator, each hole has a diameter of 14 mm and a center-to-center (c-t-c) distance of 200 mm [12]. The grid block is manufactured so that it can be attached to a treatment head similarly to an electron applicator cone.

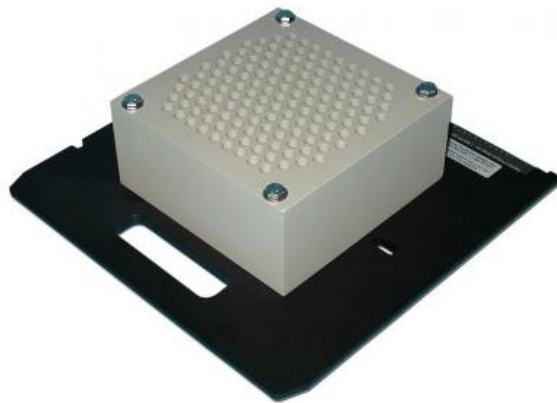


Figure 3.6 Varian Grid Block [12]

The orientations of the radial axis, the transverse axis, and the c-t-c distance are shown in Figure 3.7. The transverse axis and the radial axis are the x- and y-axes, respectively, at the face of the collimator. The c-t-c distance is the distance at isocenter between the centers of each neighboring beamlet, shown by the blue triangle. The repeated triangular unit area results in the hexagonally packed array employed in the grid collimator. The white areas represent the areas exposed directly to radiation while the gray area represents the area blocked by the Cerrobend grid collimator.

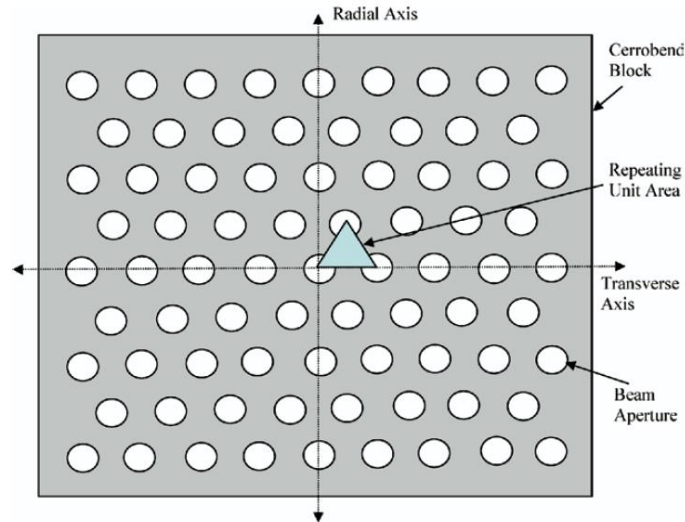


Figure 3.7 Schematic of Grid Collimator at Isocenter [5]

3.3.2 Radiobiology of X-Ray grid Therapy

In some cases, traditional radiotherapy may be limited by hypoxia within the tumor. Hypoxic cells, cells deprived of oxygen at the center of a tumor, are more radio-resistant and thus require a much higher lethal dose. At such a high dose, there is a significant risk of toxicity to normal tissue. Grid therapy delivers a single high-dose fraction to a large treatment area by collimating one broad field into several smaller fields, thus reducing the overall toxicity. Although not all of the cells are traversed by radiation due to collimation, the radiation induced bystander effect (RIBE) is evident in grid therapy [4]. RIBE occurs when cells not traversed by the radiation field exhibit a radiobiological response. The RIBE is not fully understood, but it is believed to be a response to cytokines released from neighboring radiation-traversed cells during apoptosis, programmed cell death. Because of the RIBE, even though the dose distribution is non-uniform, clinical regression of the tumor is uniform [4]. For this reason, grid therapy is used as a supplement to traditional radiation therapy for bulky untreated tumors (> 8 cm) that partially consist of radioresistant hypoxic cells [3].

The therapeutic advantage of grid therapy over traditional open field therapy is quantified in a study by Zwicker and is shown in Equation 2.

$$\text{Equation 2 [3]: } TR = \frac{S_{norm}(15 \text{ Gy grid})}{S_{norm}(5.03 \text{ Gy open})} = 1.52$$

The therapeutic ratio (TR) is the ratio of the normal tissue survival fraction in grid therapy to the normal tissue survival fraction of a reference therapy in which the same amount of tumorigenic cells are killed. The result of 1.52 in Equation 2 reveals that grid therapy results in a 52% increase in the survival fraction of normal cells. The survival fraction of a population of cells is found by using Equation 3.

$$\text{Equation 3 [3]: } S = e^{-\alpha D - \beta D^2}$$

D represents the total treatment dose, and α and β are empirical constants. For tumor cells, $\alpha = 0.289$ and $\beta = 0.0289$. For normal cells, $\alpha = 0.193$ and $\beta = 0.077$. In order to find the average survival fraction of both tumor cells and normal cells, Equation 4 is used.

$$\text{Equation 4 [3]: } S_{avg} = 0.5(e^{-\alpha_1 D - \beta_1 D^2} \cdot e^{-\alpha_2 D - \beta_2 D^2})$$

The subscript “1” denotes cell type “1” (i.e. tumor cells), and the subscript “2” denotes cell type “2” (i.e. normal cells).

The analysis of therapeutic ratio reveals that grid therapy can be designed to yield the same amount of tumor cell destruction while decreasing the resultant toxicity to normal tissues. This model of analysis is particularly robust to changes in the grid design and the percentage of tissue exposed to the beam [3].

3.4 Application of Grid Therapy to Protons

The application of grid therapy to protons is a novel idea. The SFPT model aims to achieve a similar hexagonal packed design and percent exposure to traditional grid therapy. The radiobiological characteristics of protons allow a more conformal dose distribution to the tumor

volume, thereby decreasing normal tissue toxicity. It is important to note that the following simulation is based on data from a single IBA/Varian pencil beam scanning system at Provision Proton Therapy Center in Knoxville, Tennessee. As a result, the model is not directly useful for other facilities since similar simulations performed at other institutions may render different results; however, the model serves as an analytical baseline and may be applied to another facility using its own in-house data.

CHAPTER 4: MCNP6 Model of Clinical Proton Beam

This chapter describes the virtual source-to-surface distance (SSD) setup used to create the clinical proton beam model in MCNP. Additionally, the beam geometry and dosimetric calculations, both theoretical and experimental, are discussed in this chapter.

4.1 Macroscopic Geometry in MCNP6

The MCNP6 model consists of individual proton beams incident upon a water phantom. The proton beam under investigation is 121 MeV with a Bragg peak at approximately 10.8 cm in water. The water phantom is 30 cm deep, much greater than the Bragg peak distance in water. The cross-section of the phantom is 20 cm x 20 cm to ensure that nearly all of the scattered dose is collected before escaping the phantom. The macroscopic geometry of the source and the phantom is shown in Figure 4.1.

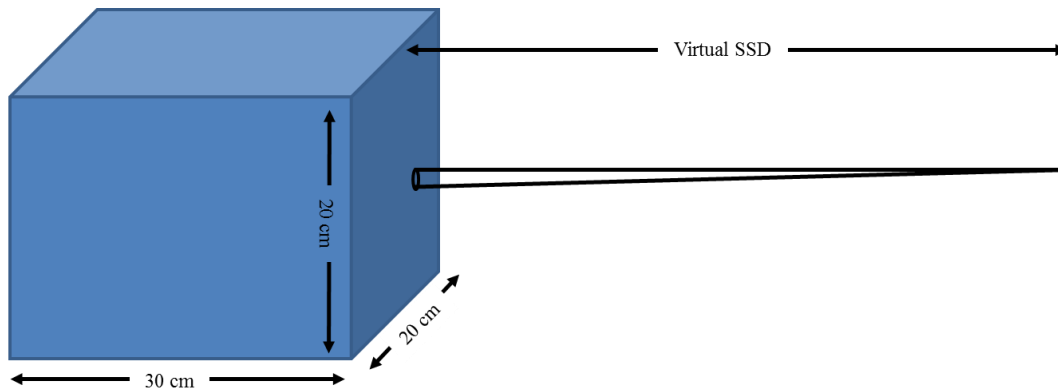


Figure 4.1: MCNP6 Macroscopic Geometry (Not Drawn to Scale)

Clinical FWHM data from Provision Proton Therapy in Knoxville, Tennessee, are shown in Table 4.1. σ_x and σ_y are clinical pencil beam standard deviations derived from the proton beam's Gaussian dose distribution. This data is for a beam on the central axis (CAX), and measurements

are conducted at varying depths in air along the CAX. For simplicity of the model, σ_{avg} , the average of σ_x and σ_y , will be used. The FWHM can be found using Equation 5.

$$\text{Equation 5: } FWHM = 2.35 \cdot \sigma_{avg}$$

Table 4.1: 121 MeV FWHM Data

<i>Distance from Isocenter (cm, - denotes towards source)</i>	σ_x (cm)	σ_y (cm)	σ_{avg} (cm)	<i>FWHM</i> (cm)
-20	0.570	0.595	0.583	1.369
-10	0.587	0.611	0.599	1.408
0	0.619	0.626	0.623	1.463
10	0.643	0.655	0.649	1.525
20	0.669	0.677	0.673	1.582

A virtual SSD method was used to define the source position since the cyclotron and bending magnet system cannot be modeled well in MCNP6. A trendline was created comparing the position along the CAX with the average standard deviation of the beam. The equation for the trendline and the correlation value are shown in Equation 6. The virtual SSD corresponds to the point at which the average standard deviation (or the FWHM) is zero, the x-intercept of Equation 6. The value of the virtual SSD is approximately 271 cm upstream from isocenter (the surface of the water phantom).

$$\text{Equation 6: } y = 0.0023x + 0.62521, R^2 = 0.994$$

The proton beams are delivered in a hexagonally packed array similarly to x-ray grid therapy. The proton beam diameter from this point forward will be defined as the FWHM of the beam. The beam diameter at isocenter is 14.6 mm, and the center-to-center distance is 280 mm. The proton grid geometry and beamlet nomenclature at isocenter are shown in Figure 4.2. The same axis nomenclature is used as that described in section 3.3.1. The plane of view in Figure 4.2 is

the plane perpendicular to the machine's CAX at the surface of the water phantom closest to the treatment head. The transverse and radial axes correspond to the in-plane x- and y-axes, respectively. Again, the c-t-c distance defines the repeated triangle unit area that creates the hexagonally packed array.

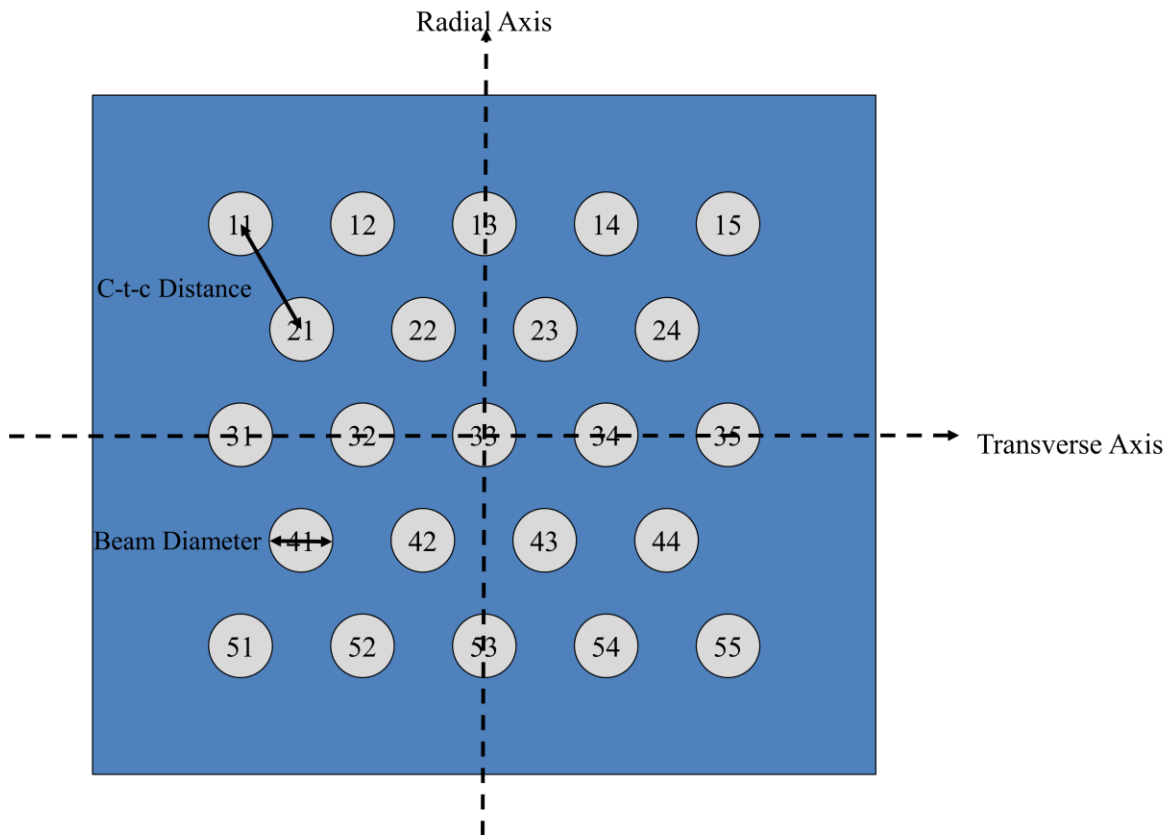


Figure 4.2: Hexagonally Packed Array of 121 MeV Proton Beams at Isocenter

4.2 Proton Beam Geometry in MCNP6

The size of the proton beam is a function of the energy, so the Gaussian model described below for 121 MeV protons must be adjusted based on the FWHM data provided for the respective proton energy. The dose distribution of the proton beam is Gaussian in nature and is modeled as such. The source card for the CAX proton beam is shown in Figure 4.3.

```

c Source
SDEF POS=-270.712275384282 0 0 ERG=121 PAR=h VEC=1 0 0 DIR=d1
SI1 -1 0.999976206 0.999980007 0.999983476 0.999986616 0.999989425
    0.999991903 0.999994051 0.999995869 0.999997356 0.999998513 0.999999339
    0.999999835 1
SP1 0 0.9999881032 0.0000019001 0.0000017349 0.0000015697 0.0000014045
    0.0000012393 0.0000010740 0.0000009088 0.0000007436 0.0000005783
    0.0000004131 0.0000002479 0.0000000826
SB1 0 0 0.011685184 0.021142753 0.035622575 0.055775775 0.080929884
    0.108387301 0.133180894 0.148697298 0.148308942 0.127657301 0.086736332
    0.030766766

```

Figure 4.3: CAX Beam Source Card

“POS=-270.71...” defines the virtual SSD of 270.71 cm, upstream from isocenter. “ERG=121” denotes the energy of the protons. “PAR=h” defines the source particle as protons. “VEC=1 0 0” defines the unit vector upon which the proton source is directed.

The source is modeled as a point source collimated into a cone of directions shown in Figure 4.4.

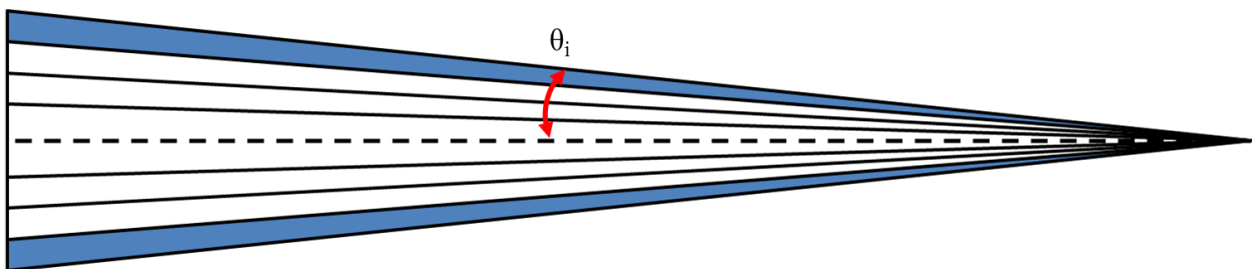


Figure 4.4: Point Source Collimated into Cone of Directions

A typical point source emits particles isotropically with equal probability of emitting a particle in any direction. By collimating the point source into several cones of directions and

adjusting the probability of particle emission into each cone, the Gaussian distribution of the proton beam can be modeled. This is accomplished through the use of the SI1, SP1, and SB1 values in the source card. The SI1 entries are the upper bin cosine limits, $\mu_i = \cos(\theta_i)$ [13]. The SP1 entries are the fractional solid angles of their respective bins, $f_{sa_i} = [(1 - \mu_{i-1}) - (1 - \mu_i)]/2$ [13]. The SB1 entries give the emission probability for each bin [13]. Each set of SI1, SP1, and SB1 values corresponds to a ring of the Gaussian distribution. In Figure 4.4, one such ring is shaded in blue. Each ring is defined at a certain radius away from the center, and the probability of emission within that ring of radius r is found using Equation 7.

$$\text{Equation 7: } P(x) = e^{-r_i/2\sigma^2} - e^{-r_{i-1}/2\sigma^2}$$

For the 121 MeV proton beam used in the MCNP model, the SI1, SP1, and SB1 values are given in Table 4.2.

Table 4.2: SI1, SP1, and SB1 Values for 121 MeV Proton Beam at Isocenter

Outer Radial Limit (cm)	SI1	SP1	SB1
∞	-1.0000000000	0	0
1.867500	0.9999762064	0.9999881032	0
1.711875	0.9999800067	0.0000019001	0.01169
1.556250	0.9999834765	0.0000017349	0.02114
1.400625	0.9999866159	0.0000015697	0.03562
1.245000	0.9999894249	0.0000014045	0.05578
1.089375	0.9999919034	0.0000012393	0.08093
0.933750	0.9999940514	0.0000010740	0.10839
0.778125	0.9999958690	0.0000009088	0.13318
0.622500	0.9999973562	0.0000007436	0.14870
0.466875	0.9999985129	0.0000005783	0.14831
0.311250	0.9999993390	0.0000004131	0.12766
0.155625	0.9999998348	0.0000002479	0.08674
0	1.0000000000	0.0000000826	0.03077

Since the virtual SSD is so large in comparison to the beam diameter, the angular difference due to the different spot locations does not affect the observed Gaussian distribution. For this reason, the same Gaussian distribution is used for all beamlets whether they are located on the CAX or not. Off-axis beam locations are achieved using the unit vector term, “VEC=...,” in the source card shown in Figure 4.3. The unit vectors for each spot are shown in Table 4.3.

Table 4.3: Unit Vectors for 121 MeV Proton Beam

Spot Number	Unit Vector		
	X	Y	Z
11	0.999625782	0.017908036	-0.020678428
12	0.99978611	0.017910908	-0.010340872
13	0.99983957	0.017911866	0
14	0.99978611	0.017910908	0.010340872
15	0.999625782	0.017908036	0.020678428
21	0.99983957	0.008955933	-0.015512138
22	0.999946515	0.008956891	-0.005171266
23	0.999946515	0.008956891	0.005171266
24	0.99983957	0.008955933	0.015512138
31	0.99978611	0	-0.020681745
32	0.999946515	0	-0.010342532
33	1	0	0
34	0.999946515	0	0.010342532
35	0.99978611	0	0.020681745
41	0.99983957	-0.008955933	-0.015512138
42	0.999946515	-0.008956891	-0.005171266
43	0.999946515	-0.008956891	0.005171266
44	0.99983957	-0.008955933	0.015512138
51	0.999625782	-0.017908036	-0.020678428
52	0.99978611	-0.017910908	-0.010340872
53	0.99983957	-0.017911866	0
54	0.99978611	-0.017910908	0.010340872
55	0.999625782	-0.017908036	0.020678428

4.3 Dose Calculation in MCNP6

Tallies are used as a way to measure a quantity in MCNP, whether that quantity is particle fluence, particle flux, or energy deposition. In this model, the end goal is to track the dose deposition at certain planes in the water phantom. Dose is defined as energy absorbed per unit mass, and its SI unit is in Gray (Gy) which is equivalent to one Joule per kilogram (1 J/kg). The planes of interest are at the surface, at the depth of the Bragg peak (10.8 cm for 121 MeV protons), and at an intermediary depth of 5 cm.

Two tallies are employed in this model: TMESH1 and TMESH3. The TMESH tally can be used to measure particle flux and dose on a cylindrical, rectangular, or spherical mesh system. In this model, a rectangular mesh is employed. Figure 4.5 shows the tally card for a TMESH1 tally.

```
c Tally
TMESH
  RMESH11:h TRAKS
  CORA11 0 1i 0.5
  CORB11 -10 199i 10
  CORC11 -10 199i 10
ENDMD
```

Figure 4.5: TMESH1 Tally Card

TMESH1 is a track-averaged mesh tally, and it measures the number of tracks, or particles, that pass through a certain cell [14]. The rectangular mesh is formed by the CORA, CORB, and CORC lines. CORA defines the thickness of the mesh. In each plane of interest, the mesh is 0.5 cm thick. CORB defines the resolution of the mesh in the y-direction. For instance, our leftward bound is -10 cm, and our rightward bound is +10 cm. The term 199i determines the number of mesh lines between the leftward and rightward bound: in this case, we will have 199 dividing mesh lines between -10 cm and +10 cm. This means that the spatial resolution in the y-direction

is 0.1 cm. CORC defines the resolution of the mesh in the z-direction in the same aforementioned manner. After all of the mesh lines have been constructed, a pattern of neighboring rectangular cells is created. The rectangular mesh results in a 200x200 array of voxels that are 0.1 cm by 0.1 cm by 0.5 cm. The TMESH1 tally measures the number of tracks, or particles, passing through each cell created by the mesh.

The TMESH3 tally works in the same way; however, instead of measuring the number of tracks passing through each cell, it measures the energy deposition in each cell from all particles [14]. This eliminates the need to calculate primary and secondary dose since all forms of dose deposition are considered in this tally. The way in which the TMESH3 tally measures dose deposition is by calculating the difference between the entrance energy and the exit energy for each mesh. The output is in terms of energy deposited per unit volume per source particle ($\text{MeV}/\text{cm}^3/\text{source particle}$). In order to calculate the absolute dose deposited per volume, the result of the TMESH3 tally must be multiplied by the result of the TMESH1 tally in each respective cell. The result of this operation provides the end goal of energy deposition per unit volume, which gives the absorbed dose.

One million particle histories are recorded for each beam. Each beam's run time is approximately 20 minutes. This is performed for beams 11, 12, 13, 21, 22, 31, 32, 33. Instead of performed the same lengthy simulations for the remaining beams. They are just treated as a mirror image of the original eight beams. All of the beams are then overlaid on the same phantom plane using MATLAB. A smoothing function is applied to the MCNP6 results in MATLAB. It is a 5x5 box filter. The smoothing function sets each pixel value to the mean value of the 5x5 pixel square around it. Since all of the cells in the mesh are the same volume,

normalization is relatively simple. All results are normalized to the maximum dose in their respective plane of interest (i.e. at the surface, at 5 cm depth, or at 10.8 cm depth).

4.4 Dose Calculation in RayStation

RayStation is a commercially available that allows dose calculation from photon, electron, and proton radiotherapy treatments [15]. In this study, RayStation is used to mimic and validate the dose distribution from the MCNP6 model. The phantom model in the RayStation simulations has the same macroscopic characteristics as the MCNP6 model. The spot positions of the beamlets are also the same as those determined by the directional unit vectors in Table 4.3 for the MCNP6 model. Additionally, the dose in RayStation is analyzed at the same planes of interest as the MCNP6 model: 0 cm, 5 cm, and 10.8 cm. The maximum dose from each beam is 75 cGy which corresponds to approximately 5 monitor units per beam. The dose is normalized to the in-plane maximum dose.

Calculation of proton dose is performed by RayStation's pencil beam dose algorithm. The algorithm utilizes the characteristics of the lateral and longitudinal proton fluence as well as integrated depth dose components [15]. The fluence description is derived from a number of beam model parameters: energy spectrum, angular distribution moments at isocenter, virtual source axis distance, and range modulation steps if the range modulator wheel is employed [15]. These characteristics create the phase space parameters which are transported through the patient along the CAX of the beam. Energy loss is modeled using the Bethe-Bloch stopping power expression, and the Fermi-Eyges theory predicts the spatial and angular distribution of the beam at any depth in air or in the patient.

4.5 Experimental Setup and Dose Measurement Using Gafchromic EBT3 Film

Gafchromic EBT3 film is a dosimetry technique used to verify a treatment plan for use on a patient. The film is made of a radiosensitive organic material. In the presence of radiation, the film turns blue, and the darkness of the film increases with increasing radiation. No treatment of the films is required to fix the dose deposition before being read. The films are typically placed between solid water phantoms to mimic the presence of patient tissue. In this experiment, Gammex solid water is used.

The experimental setup in order from the bottom (surface of the couch) to the top (surface closest to the beam) is 5 cm thick solid water slab, film 3, 2 mm solid water slab, 3 mm solid water slab, 5 cm solid water slab, film 2, 5 cm solid water slab, film 1. This setup is shown in Figure 4.6.

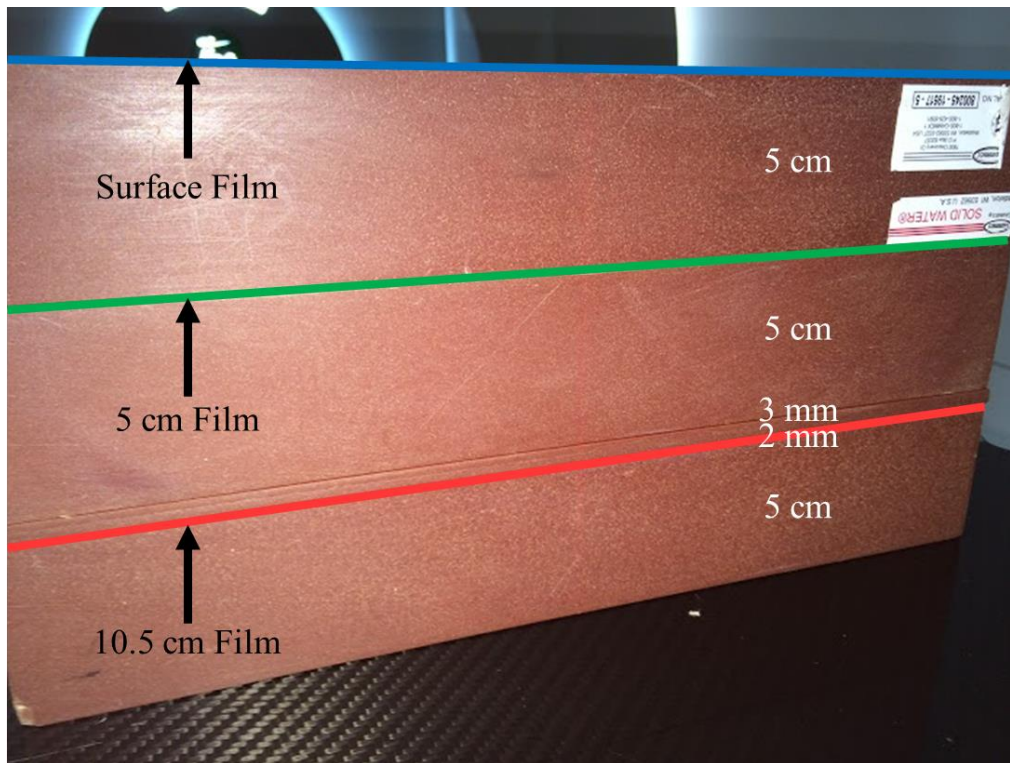


Figure 4.6: Experimental Setup of Solid Water and Gafchromic EBT3 Films

Film 1 is located at the surface of the phantom and corresponds to the surface measurements calculated in MCNP6 and RayStation. Film 2 is located at a depth of 5 cm and corresponds to the 5 cm measurements calculated in MCNP6 and RayStation. Since the depth in actual water is treated as 1.025 times the depth in solid water, film 3 is measured at a depth of 10.5 cm in solid water, which corresponds to approximately 10.8 cm, the depth of the Bragg peak.

The stack of solid water slabs and films was aligned laterally with lasers, and then the couch was raised so that the top of the stack was at machine isocenter. Laser localization was used to verify the setup. 40 monitor units were delivered to each spot giving a maximum dose point of approximately 6 Gy. This dose was chosen for its good visibility and limited noise levels on the film. A 5x5 smoothing function was applied using OmniProRT software. The smoothing function sets each pixel value to the mean value of the 5x5 pixel square around it. Just as in the MCNP6 and RayStation simulations, the dose is normalized to the in-plane maximum dose.

CHAPTER 5: MCNP6, RayStation, and Experimental Results

5.1 MCNP6 Results

5.1.1 Percentage Depth Dose

In order to identify the depth of the Bragg peak, a simulation was performed in MCNP6. The macroscopic geometry is the same as that described in 4.1; however, the dose profile is only created for the CAX beam. 500,000 particle histories were tracked with a run time of 22.37 minutes. The water phantom was divided up into 0.05 cm thick planes from the surface of the water phantom to a depth of 13 cm, which is beyond the estimated depth of the Bragg peak. The planes run perpendicular to the CAX of the beam. Between each plane and within the confines of the water phantom a cell is created. In each cell a *F8 tally is performed measuring the total energy deposition in the cell, similarly to the TMESH3 tally. The results of the *F8 tally are in the same units as the TMESH3 tally, (MeV/cm³/source particle). In order to get the energy deposited per volume of each cell, the results of the *F8 tally were multiplied by the number of particles traversing each cell, the same process as the calculation of dose using the TMESH1 and TMESH3 tallies. The results of the simulation are normalized to the maximum dose along the CAX. The depth of the Bragg peak is 10.8 cm, and the results from the simulation are shown in Figure 5.1. This measurement defines the plane of interest at depth which is investigated in the MCNP6, RayStation, and Gafchromic film simulations. As mentioned earlier, measurements of the dose profile are also taken at the surface of the water phantom as well as at an intermediary depth of 5 cm.

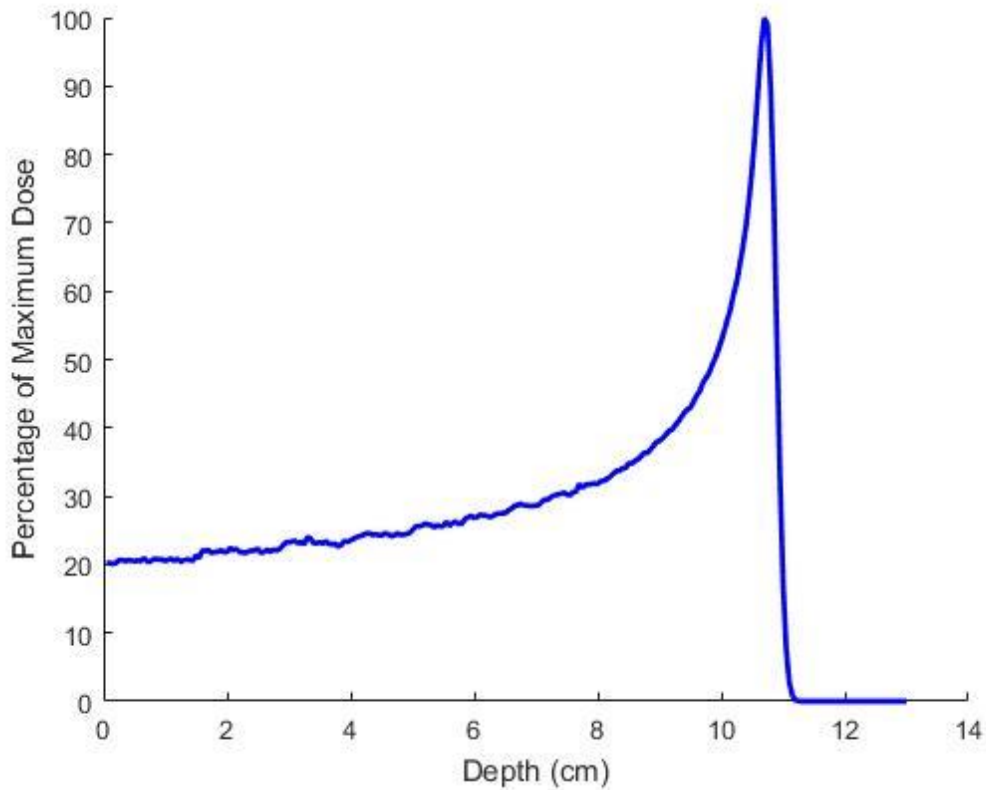


Figure 5.1: Percentage Depth Dose for 121 MeV Protons

5.1.2 Gaussian Beam Profile

As described in section 4.2, the proton beam is modeled as a point source collimated into a cone of directions. This allows the source to have a Gaussian-like shape both in particle distribution and dose deposition. Using the data provided from Provision Proton Therapy, the FWHM at the surface of the water phantom was determined to be 14.6 mm. Using this information and the analysis described in section 4.2, the Gaussian profile for the CAX beam was acquired and is shown in Figures 5.2 and 5.3.

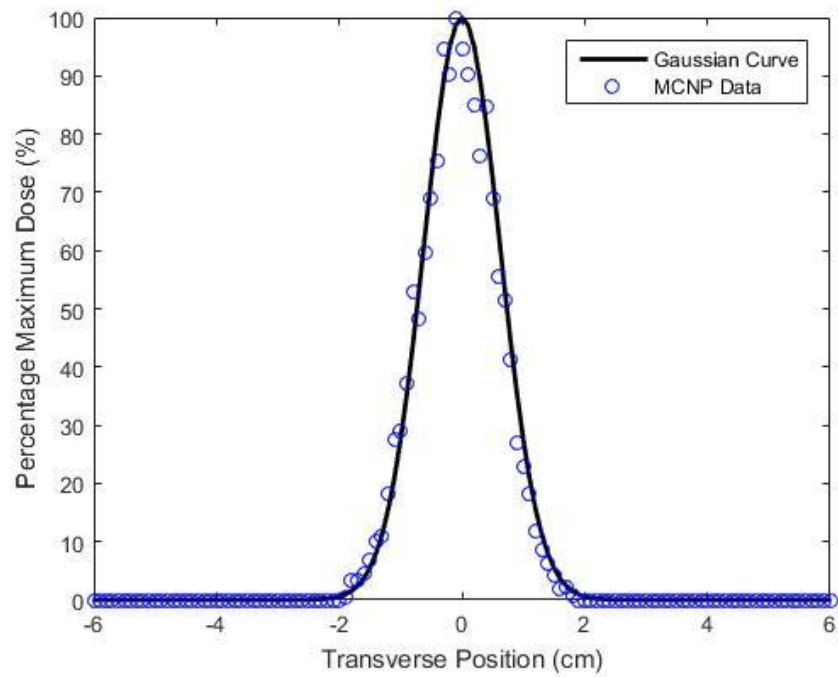


Figure 5.2: Transverse Profile of CAX Beam at Surface of Water Phantom

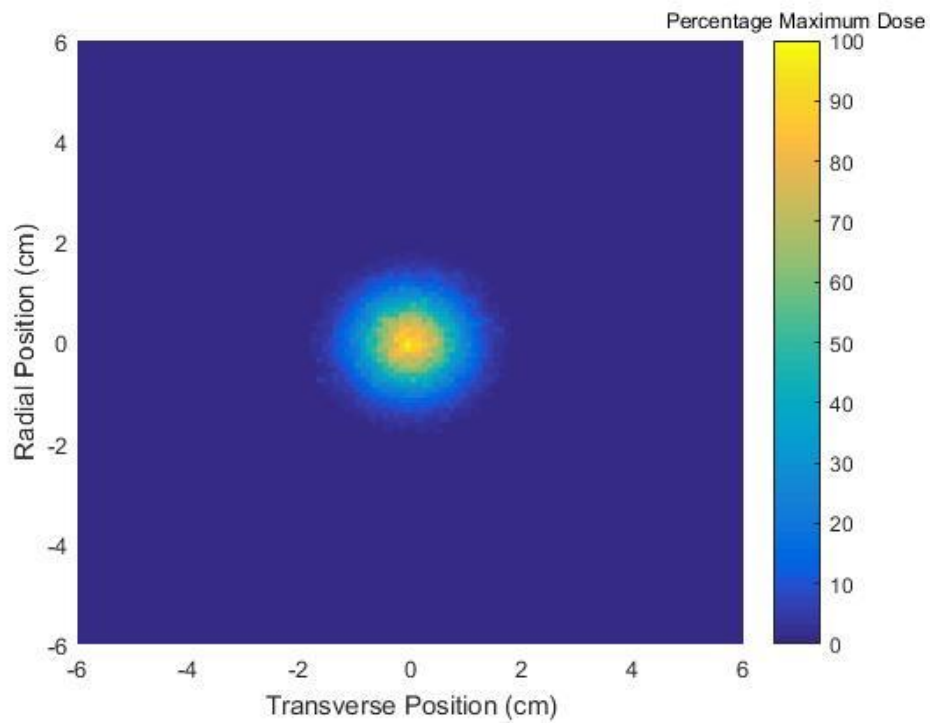


Figure 5.3: Dose Distribution of the CAX Beam at the Surface of the Water Phantom

This model and all further MCNP models utilize the TMESH1 and TMESH3 tally calculations discussed in Chapter 4. Figure 5.2 shows the transverse profile of the CAX beam at the surface of the water phantom. The blue dots denote the approximation of the Gaussian distribution created by the point source collimated into a cone of directions. The root mean square difference between the two sets of data is 2.08% meaning that the uncertainty of the model is small compared to the size of the model. Since the size of the SSD is much larger than the width of the proton beam, the Gaussian probability distribution is not adjusted for off-axis beams. Figure 5.3 shows the in-plane dose distribution at the surface of the water phantom for the CAX beam. The average relative error for the entire dose distribution is $2.0961 \cdot 10^{-5}$. This is much smaller than the recommended MCNP relative error cutoff of 0.1, indicating that the number of particles and the employed mesh adequately measure the dose distribution with good certainty.

5.1.3 Spatially Fractionated Proton Dose Distributions

The in-plane dose distributions at the surface of the water phantom, at an intermediary depth of 5 cm, and at the depth of the Bragg peak (10.8 cm) are shown in Figure 5.4. The relative error of the dose profiles at the surface, at 5 cm depth, and at 10.8 cm depth are $2.1506 \cdot 10^{-5}$, $4.3602 \cdot 10^{-4}$, and $6.2425 \cdot 10^{-4}$, respectively.

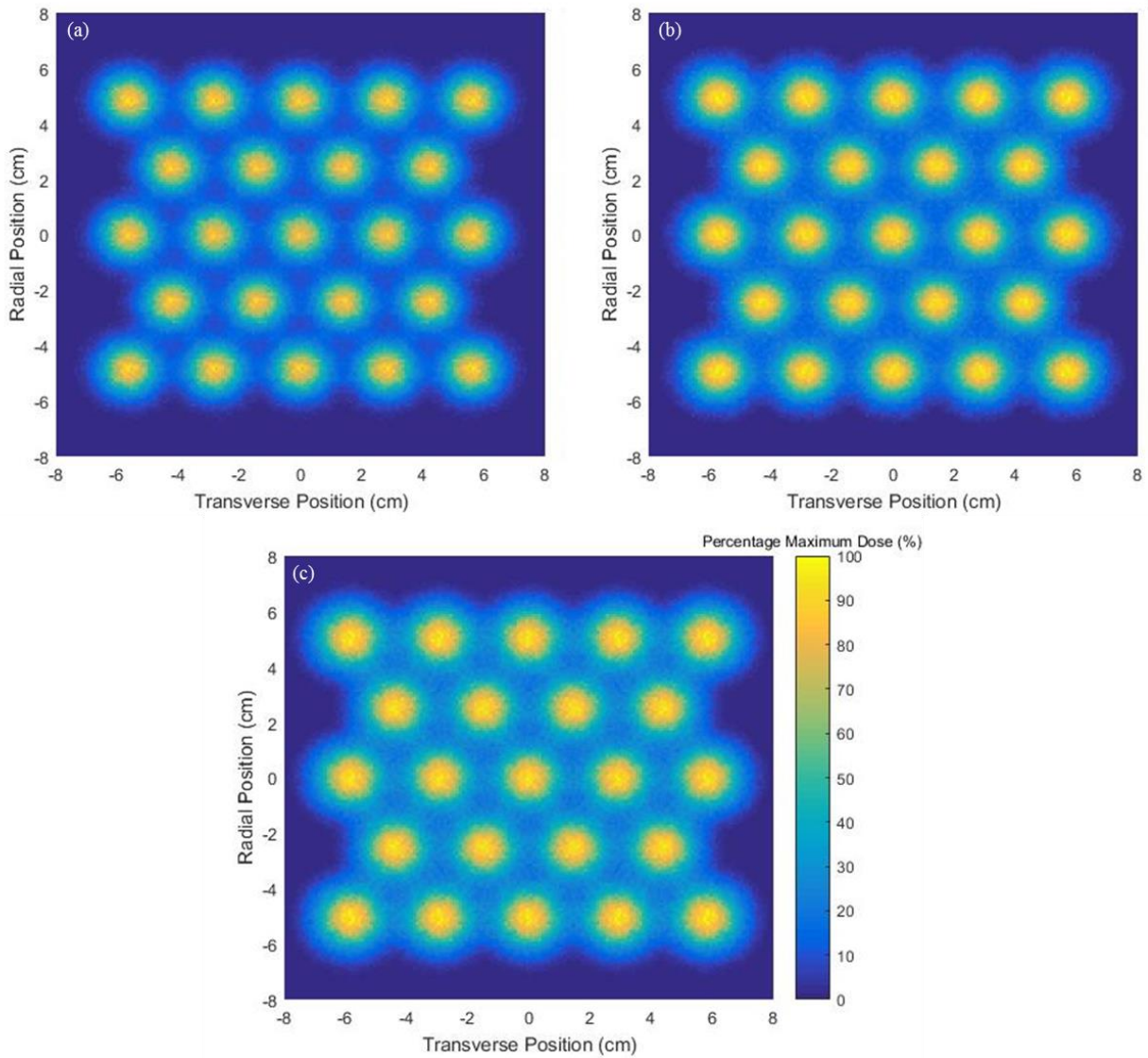


Figure 5.4: MCNP6 Dose Distribution at (a) Surface, (b) 5 cm, (c) 10.8 cm

An observed effect from the surface to the depth of the Bragg peak is a widening of the grid field. This is primarily due to the divergence of off-axis beams as they traverse through the phantom. It is most evident when observing the central locations of corner beamlets. These locations are shown in Table 5.1. The divergence due to off-axis beams follows a linear trend as expected.

Table 5.1: Corner Beamlet Locations

Surface			5 cm			10.8 cm		
Beamlet Number	Transverse Position (cm)	Radial Position (cm)	Beamlet Number	Transverse Position (cm)	Radial Position (cm)	Beamlet Number	Transverse Position (cm)	Radial Position (cm)
11	-5.7	4.8	11	-5.8	4.9	11	-5.9	5.2
15	5.6	4.8	15	5.7	4.9	15	5.8	5.2
51	-5.7	-4.9	51	-5.8	-5	51	-5.9	-5.3
55	5.6	-4.9	55	5.7	-5	55	5.8	-5.3

Another important feature of the dose profiles is characterized by the divergence and scatter of the protons within the beam. This is quantitatively observed through the increase in the FWHM of the beam as it traverses through the water phantom. The FWHM's of the central axis beam at the surface, at 5 cm depth, and at 10.8 cm depth are 1.5001 cm, 1.5873 cm, and 1.7479 cm, respectively. The divergence and scatter of the protons within a single beam also follows a linear trend.

The off-axis divergence and the in-beam divergence both contribute to the degradation of the peak-to-valley dose ratio (PVDR) as the beams travel through the water phantom. This effect can be seen in Figure 5.5.

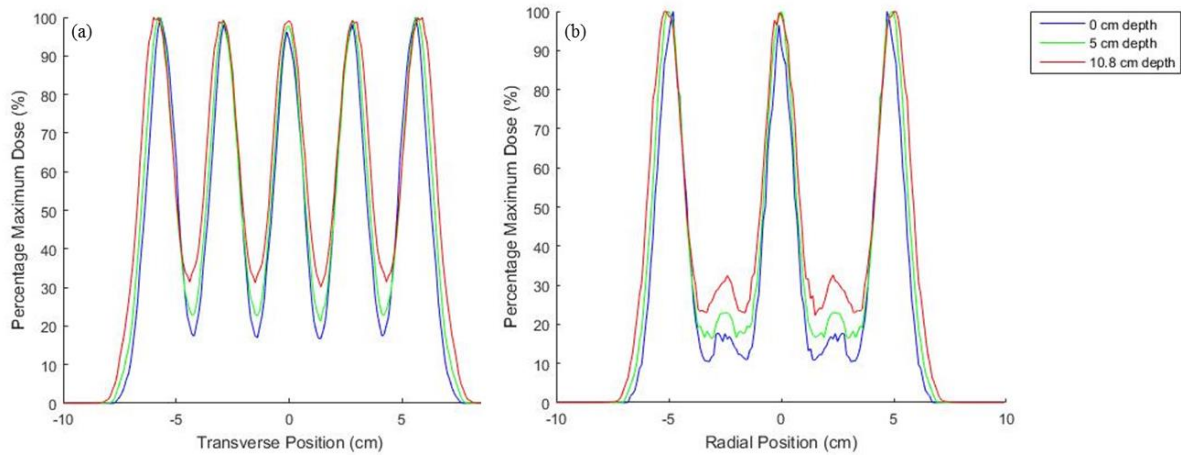


Figure 5.5: MCNP6 (a) Transverse and (b) Radial Dose Profiles

The PVDR's for both the transverse and lateral profiles are calculated off of these figures. The transverse and radial profiles have distinctly different characteristics creating the need to calculate the PVDR's differently. For the transverse profile, the PVDR is the ratio of the average maximum beamlet dose to the average of the valley dose. For the radial profile, the PVDR is the ratio of the average maximum beamlet dose to the average of the maximum dose located within each valley. Table 5.2 shows the values for the transverse and radial profile PVDR's at the surface, at 5 cm depth, and at 10 cm depth.

Table 5.2 MCNP6 Radial and Transverse PVDR's

	Surface	5 cm	10.8 cm
Radial PVDR	5.5709	4.3365	3.0667
Transverse PVDR	5.7348	4.4355	3.2076

5.2 Comparison of MCNP6 and RayStation Results

The in-plane dose distributions acquired from the RayStation outputs have the same qualities as the MCNP6 outputs shown in Figure 5.4. They have the same resolution of 0.1 cm.

RayStation also verified the theoretical depth of the Bragg peak at 10.8 cm from the MCNP6 simulations. A comparison of the transverse profiles between the MCNP6 and RayStation outputs in Figure 5.6 shows that the Monte Carlo results better matches that of Raystation at the depth of the Bragg peak as compared to the surface. The trend is shown through the observation of the difference in the valleys between the MCNP6 and RayStation data as the beam progresses through the water phantom.

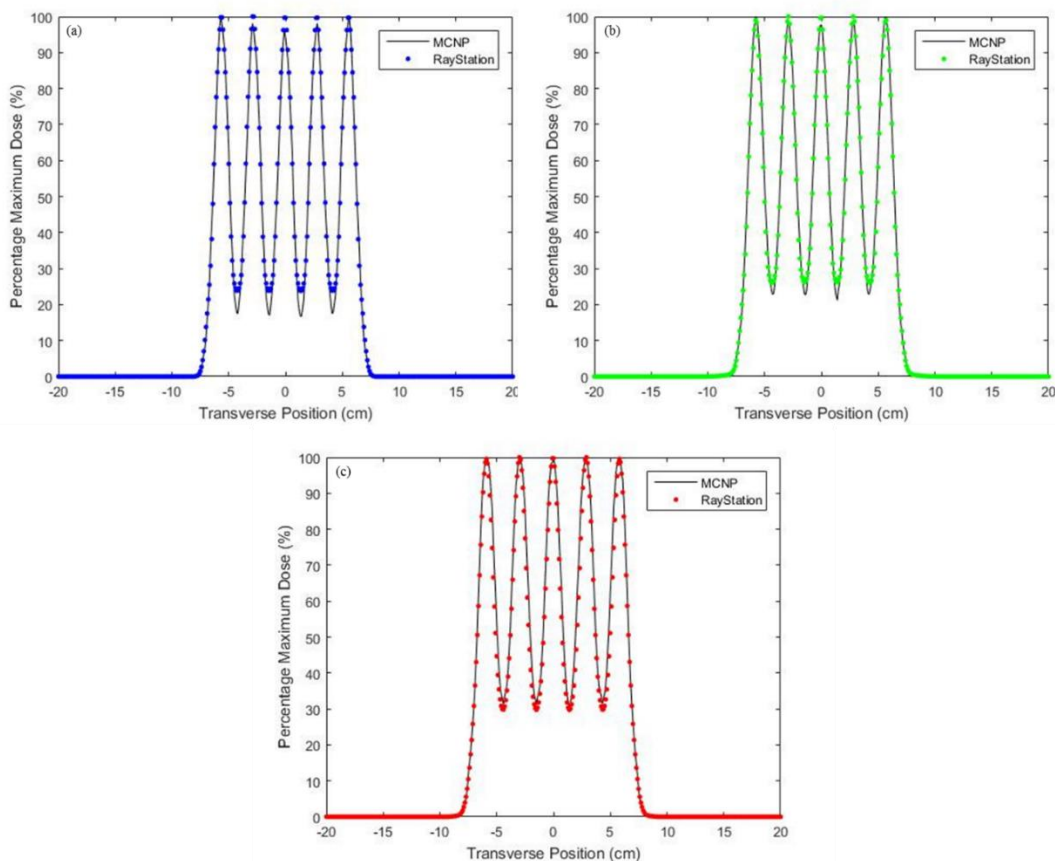


Figure 5.6: MCNP6 and RayStation Transverse Profiles at (a) Surface, (b) 5cm, and (c) 10.8 cm

One possible reason that there is a discrepancy between the dose in the valleys at the surface of the water phantom is due to a simplification of the MCNP6 model. The model assumes no photon or electron contamination from the treatment head. It would then be expected that the simulated PVDR's closer to the surface would be higher than those modeled in RayStation. A similar trend is also shown in another study that aims to dosimetrically validate megavoltage x-ray grid therapy [5]. The radial and transverse PVDR's from the RayStation outputs are shown in Table 5.3. This expectation does indeed hold true close to the surface. The MCNP6 output for the transverse PVDR is 5.7348, significantly higher than the corresponding value from RayStation, 4.1834. At the Bragg peak, there is much higher agreement between the MCNP6 and the RayStation transverse and radial PVDR's.

Table 5.3: RayStation Radial and Transverse PVDR's

	Surface	5 cm	10.8 cm
Radial PVDR	4.1677	3.7752	3.3329
Transverse PVDR	4.1834	3.8109	3.3479

In order to fully compare the in-plane dose distributions between MCNP6 and RayStation, a gamma analysis was performed. It has been shown that for pencil beam spot scanning systems, the ideal dose difference and distance-to-agreement (DTA) criteria are $\pm 3\%$ and ± 3 mm, respectively, with a pass rate cutoff of 90% [16]. Using the listed criteria, the dose profile at the surface, at 5 cm, and at 10.8 cm all met the pass cutoff with passing percentages of 92.57%, 99.0625%, and 99.99%, respectively. The gamma index plots for each in-plane comparison are shown in Figure 5.7. This trend of increasing pass percentages with increasing depth, in addition

to the observation of the PVDR trend, further verifies the agreement between the MCNP6 and RayStation outputs, especially at the depth of the Bragg peak.

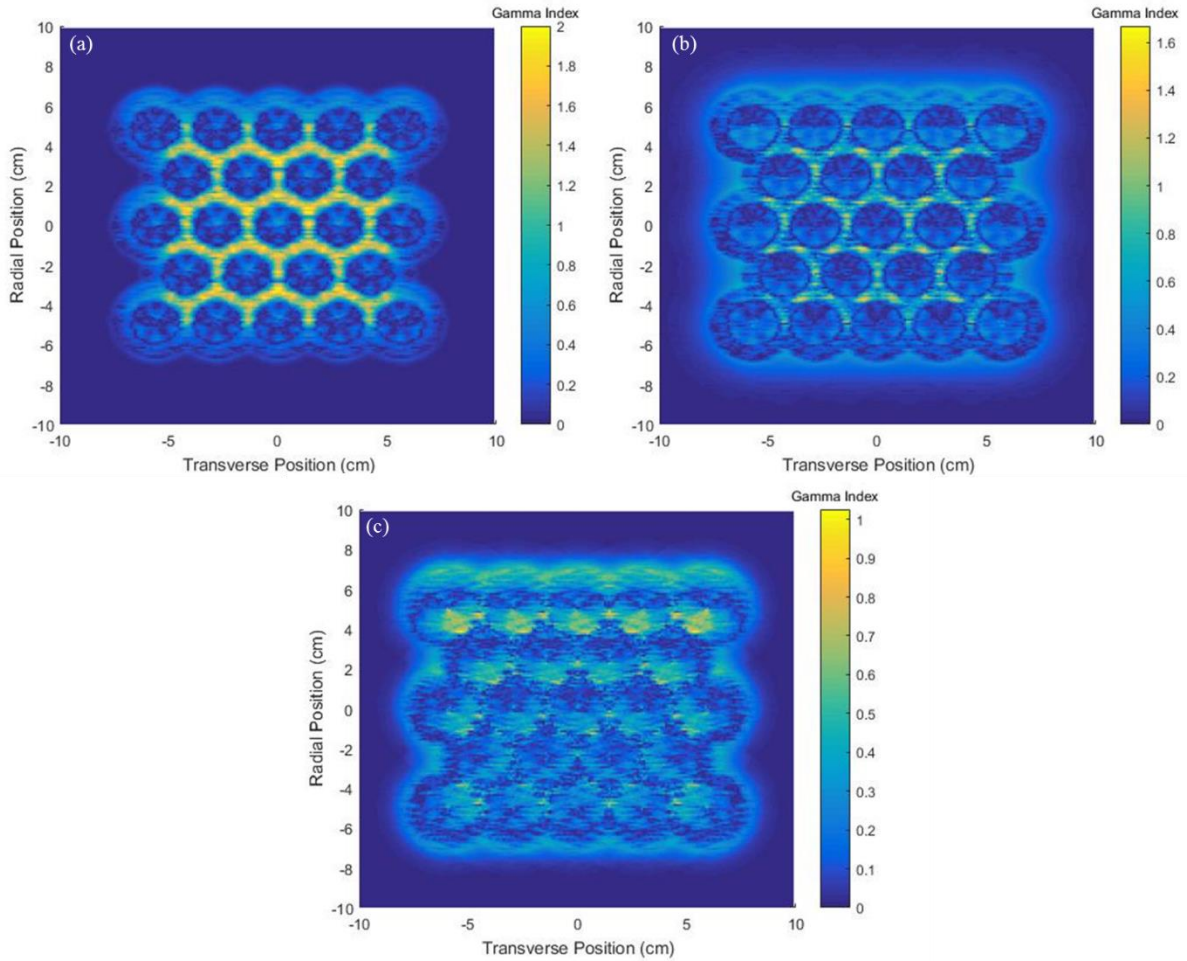


Figure 5.7: Gamma Analysis between MCNP6 and RayStation at (a) Surface, (b) 5cm, and (c) 10.8 cm

5.3 Comparison of MCNP6 and Gafchromic Film Results

Gafchromic EBT3 film was used to experimentally validate the delivery of the proton grid distribution. An image of the resultant films from the experimental setup discussed in section 4.5 is shown in Figure 5.8.

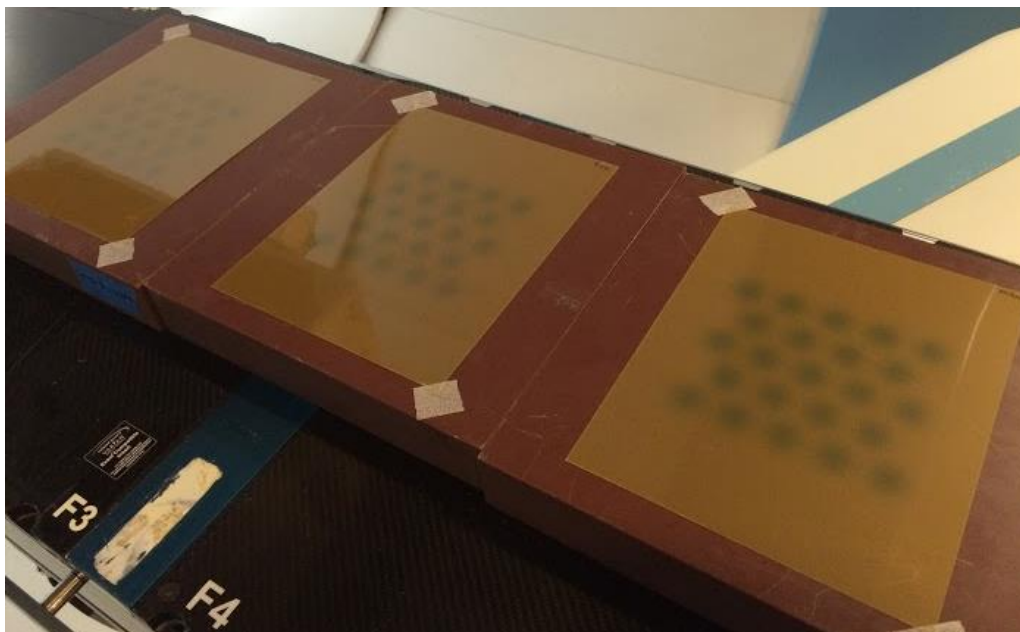


Figure 5.8: Gafchromic EBT3 Films Post-Irradiation

Upon scanning the films, a significant amount of noise was detected. The pattern does not appear to be due to the physical dose distribution of the proton grid or to the film itself, so it is attributed to the scanner. Figure 5.9 shows the in-plane dose distribution at the surface of the water phantom for the Gafchromic film after processing, and Figure 5.10 shows the radial profile of the pre- and post-processed film data. All of the data at the surface, at 5 cm, and at 10.8 cm exhibit the same linear shift as a function of radial position. In order to counteract this effect, a linear shift was performed to correct the data. This was done by an average alignment of the

valley dose values and the peak dose values which are expected to be the same among each group. Once that correction was done, a correction was performed to zero out the data – in order to eliminate the negative dose values, an effect of the noise imparted by the scanner. The results of this processing are shown in Figure 5.10.

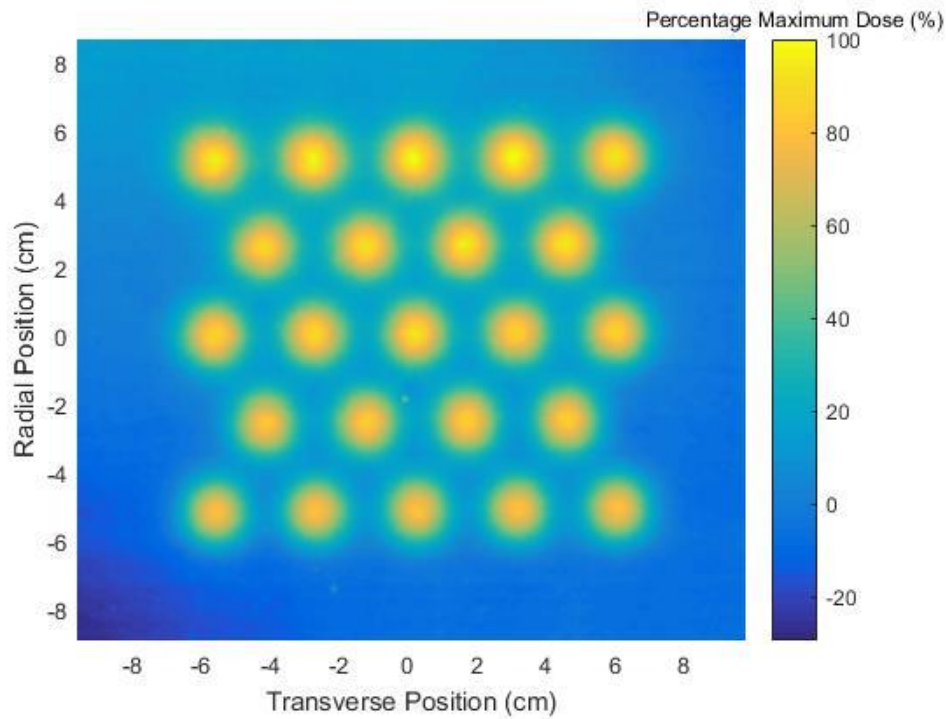


Figure 5.9: Gafchromic Film Dose Distribution at 10.8 cm Post-Processing

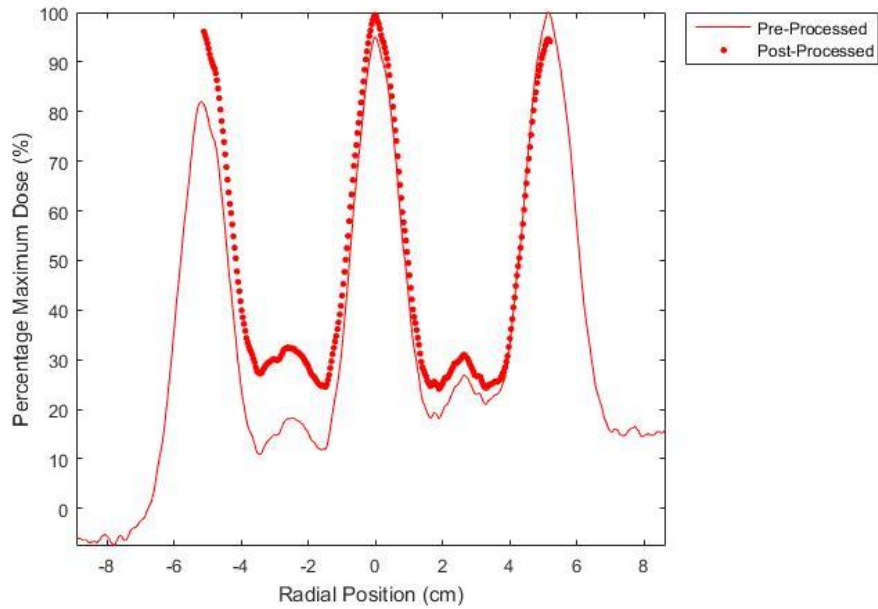


Figure 5.10: Gafchromic Film at 10.8 cm Before and After Processing

Although the data was corrected for these linear shifts, only the central component of the data could be used due to drastic falloff at the edges of dose distribution – again attributed to the film scanner. For this reason, only transverse PVDR calculations were performed due to the limited number of peaks and valleys accessible in the radial direction. The PVDR's for the surface, 5cm, and 10.8 cm are 6.8072, 6.3151, and 4.3972, respectively. The fits of each transverse profile to the corresponding MCNP6 profile are shown in Figure 5.11.

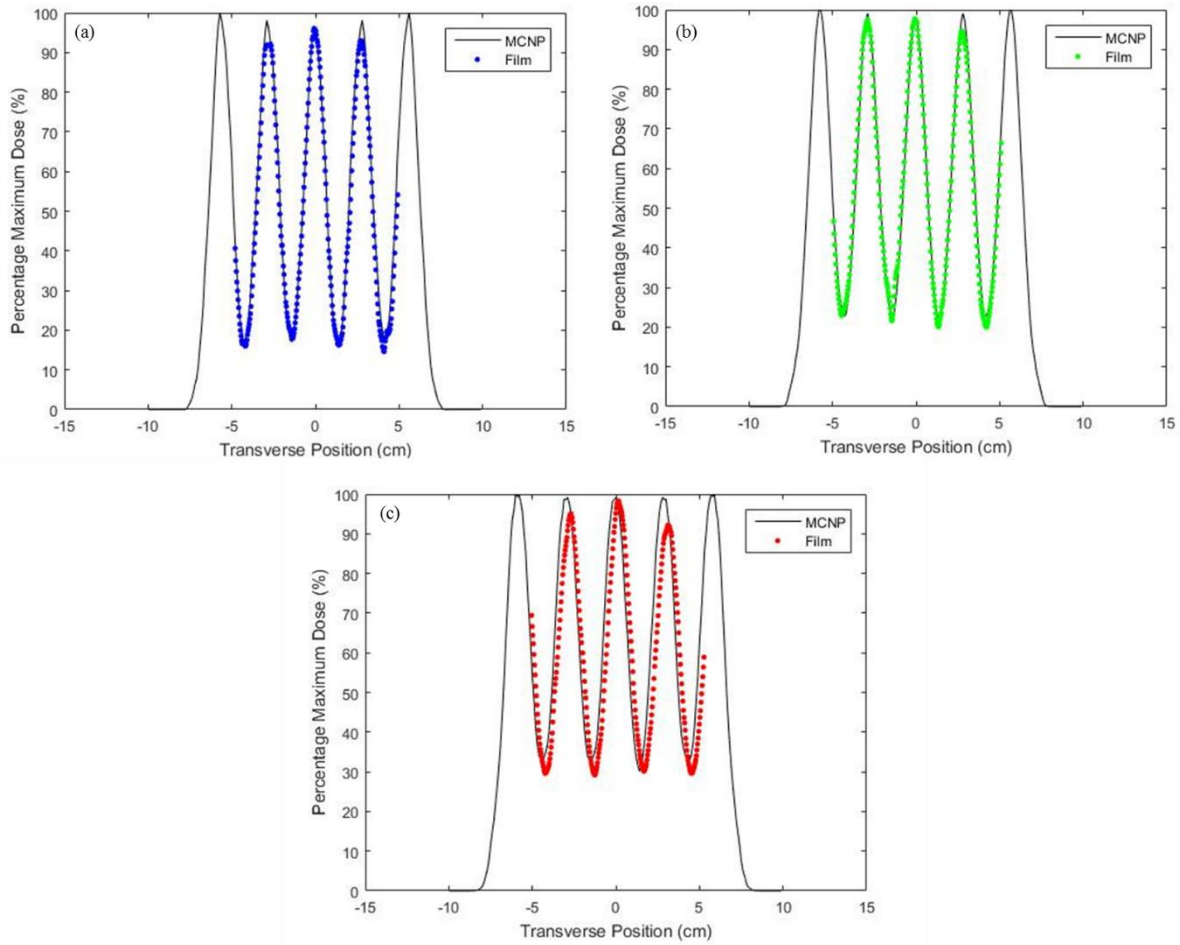


Figure 5.11: MCNP6 and Gafchromic Film Transverse Profiles at (a) Surface, (b) 5 cm, and (c) 10.8 cm

Again, a gamma analysis was used to validate the comparison of the MCNP6 and the Gafchromic film dose distributions. Due to the limitation on analyzable field size for the Gafchromic film, the gamma analysis was only performed on the central portion of both dose distributions. The same criteria were applied as in the comparison between the MCNP6 and RayStation data. The percent pass rates surpassed the cutoff of 90% for the surface, 5cm, and 10.8 cm with 98.2419%, 99.4633%, and 99.6367%, respectively. These results are shown in Figure 5.12, and they again show the excellent fit of the model to the experimental data.

Additionally, a gamma analysis was performed at 10.8 cm comparing the RayStation and the film data and resulted in a passing percentage of 97.3599%.

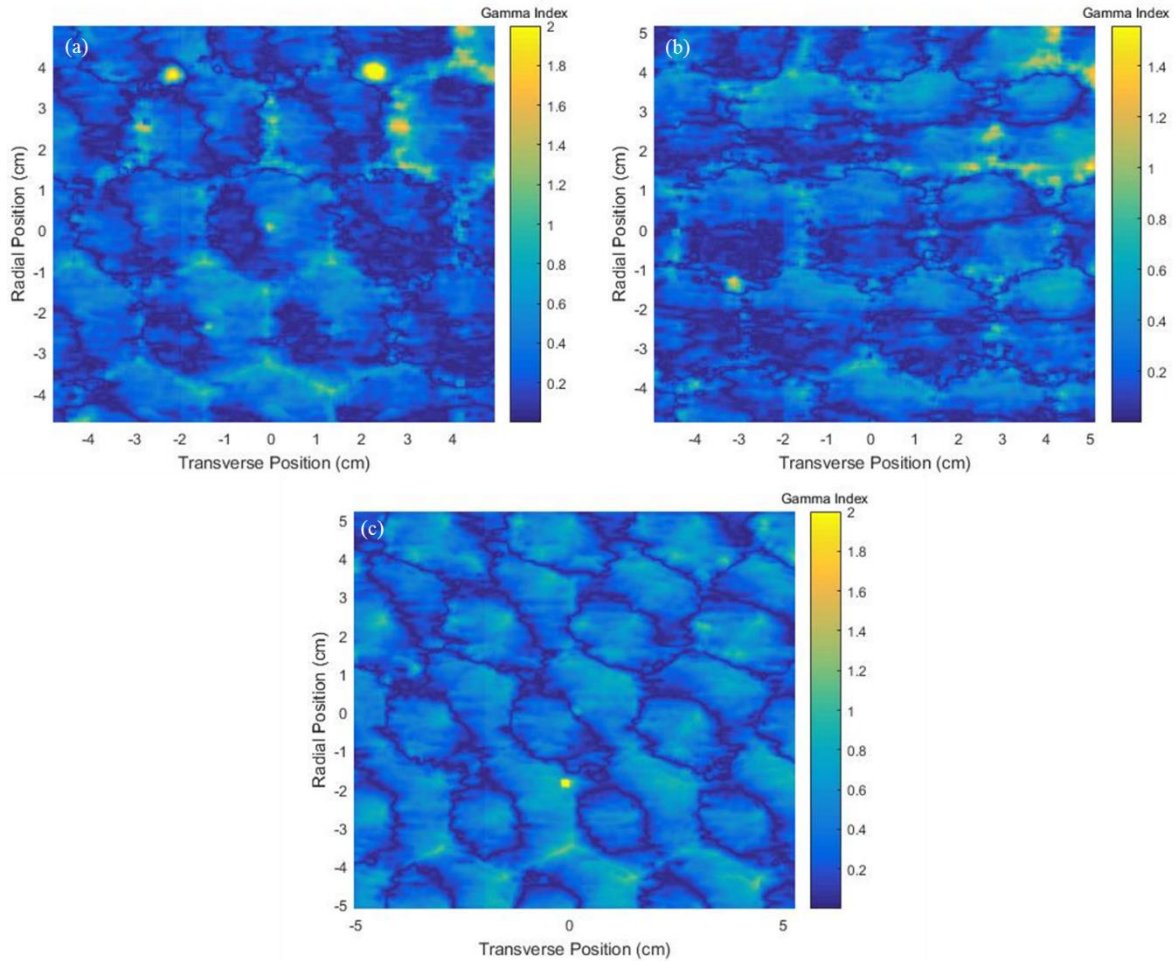


Figure 5.12: Gamma Analysis between MCNP6 and Gafchromic Film at (a) Surface, (b) 5cm, and (c) 10.8 cm

5.4 Comparison of Spatially Fractionated Proton Therapy to Photon Grid Therapy

The MCNP6 model, the RayStation results, and the processed Gafchromic film results all have excellent agreement among one another. More importantly, the new proton grid distribution is a close match to the dose distribution of photons. The beam diameters are very

similar: 14 mm for the photon grid and 14.6 mm (FWHM) for the proton grid. The c-t-c distances have a little more variation (200 mm for photon grid and 280 mm for photon grid) yet not enough to change the benefits observed quantitatively through the therapeutic ratio. The increased c-t-c distance is due to the wider Gaussian distribution of the proton beams as opposed to the finite-edge collimation in photon grid therapy.

One of the biggest benefits of using protons instead of photons in grid therapy is the survivability of the PVDR at increased depths. In photon grid therapy there is an observed decrease in the PVDR as the measurement depth increases [17]. Although the PVDR has slight degradation as the proton grid progresses through the water phantom, the PVDR survives very well up to the depth of the Bragg peak. This allows delivery of grid dose to further depths than in photon grid therapy.

For high energy protons (energy greater than 50 MeV), cell survival curves are similar to those of megavoltage x-ray. Because of these similarities, the α/β ratio employed in the linear quadratic model is similar for both types of radiation. In Chapter 2, Zwicker's study of the therapeutic ratio for grid therapy was discussed. Since the α/β ratio is the same and the percentage directly exposed to radiation is the same (50%), his study holds true for this model as well; therefore, the proton grid distribution maintains at least the same therapeutic ratio. Since protons have an RBE greater than one (≥ 1.1), it is hypothesized that the proton grid distribution will actually have a higher therapeutic ratio as compared to open field photon treatments upon experimentation [6].

CHAPTER 6: Conclusions and Future Work

6.1 Conclusions

The objective of this work was to model spatially fractionated proton therapy in MCNP6 in order to evaluate its dosimetric qualities in comparison with megavoltage x-ray grid therapy. Ultimately, this model will enable the use of spatially fractionated proton therapy in a clinical environment.

In this work, a detailed model of a clinical proton beam was constructed using data provided by Provision Proton Therapy. The approach to constructing the Gaussian beam profile as well as defining the virtual SSD allow great simplifications to reality; however, these simplifications do not impact the overall ability of the model to accurately predict reality. Tallies were used in the MCNP6 model to determine the dose delivered at several depths, and these tallies were validated with treatment planning system data as well as experimental film data. A gamma analysis was performed between each pair of data (MCNP6, RayStation, and Gafchromic film), and all of the analyses passed. These calculations confirmed the validity of the model and its usefulness in not only modeling an individual proton beam, but also in modeling an entire spatially fractionated proton dose distribution.

There were two main points of interest in this work. The first was the validation of the model using treatment planning system and experimental film data, all of which showed excellent agreement. The second, and more clinically relevant, point of interest was that the spatially fractionated proton dose distribution showed marked dosimetric advantages when compared to megavoltage x-ray grid therapy. In more ways than one, this proved to be true. The PVDR of the spatially fraction proton therapy treatment was more robust to degradation with increasing

depth in the case of protons. Additionally, the RBE leads one to believe that radiobiological experimental validation will show that the therapeutic ratio is also higher than that of x-ray grid therapy due to the similar grid geometry yet decreased dose to normal tissue. This is extremely important considering the crux of grid therapy is in the argument of increased therapeutic ratio.

Overall, a method for accurately modeling clinical proton beams as well as a method for creating a grid geometry with those beams in MCNP6 was developed. This model allows the assessment of spatially fractionated proton therapy, a technique which is not yet employed in the clinic, but one that shows very promising radiobiological results. This model was developed to model a real-world treatment in the simplest and most accurate manner possible. Although this model shows excellent agreement, future simulations and experimentation on spatially fractionated proton therapy are needed before implementation in the clinic.

6.2 Recommended Future Work

The aforementioned results establish a baseline methodology for modeling and understanding the dosimetric qualities of spatially fractionated proton therapy; however, there were several issues identified that warrant further research or experimentation.

The largest issue and one that can be easily fixed was the experimental measurement of dose using Gafchromic EBT3 film. The scanned films exhibited significant imparted error (i.e. not error from the therapy system or the film). Preferably, a two dimensional diode detector array would be used for measurement of dose, eliminating the uncertainties that come with film measurement and scanning.

Another suggestion for future work is the modeling of a grid SOBPs setup. In reality, the tumor will not lie in one plane – rather, it will span a finite depth. In order to fully understand and predict the therapeutic ratio for spatially fractionated proton therapy, three-dimensional

dosimetry needs to be performed on a proton grid SOBPs setup. Radiobiological cell culture studies would also be useful in determining the survival fraction of normal and tumor cells after proton grid irradiation. The resolution of these issues will truly allow this model to be a useful predictive tool for the implementation of spatially fractionated proton therapy in the clinical environment.

APPENDIX A: MCNP INPUTS

A.1 MCNP6 PDD Input

```
Proton beam
c Cell card
1 100 -1 -1 3 -4 IMP:h=1
2 100 -1 -1 4 -5 IMP:h=1
3 100 -1 -1 5 -6 IMP:h=1
4 100 -1 -1 6 -7 IMP:h=1
5 100 -1 -1 7 -8 IMP:h=1
6 100 -1 -1 8 -9 IMP:h=1
7 100 -1 -1 9 -10 IMP:h=1
8 100 -1 -1 10 -11 IMP:h=1
9 100 -1 -1 11 -12 IMP:h=1
10 100 -1 -1 12 -13 IMP:h=1
11 100 -1 -1 13 -14 IMP:h=1
12 100 -1 -1 14 -15 IMP:h=1
13 100 -1 -1 15 -16 IMP:h=1
14 100 -1 -1 16 -17 IMP:h=1
15 100 -1 -1 17 -18 IMP:h=1
16 100 -1 -1 18 -19 IMP:h=1
17 100 -1 -1 19 -20 IMP:h=1
18 100 -1 -1 20 -21 IMP:h=1
19 100 -1 -1 21 -22 IMP:h=1
20 100 -1 -1 22 -23 IMP:h=1
21 100 -1 -1 23 -24 IMP:h=1
22 100 -1 -1 24 -25 IMP:h=1
23 100 -1 -1 25 -26 IMP:h=1
24 100 -1 -1 26 -27 IMP:h=1
25 100 -1 -1 27 -28 IMP:h=1
26 100 -1 -1 28 -29 IMP:h=1
27 100 -1 -1 29 -30 IMP:h=1
28 100 -1 -1 30 -31 IMP:h=1
29 100 -1 -1 31 -32 IMP:h=1
30 100 -1 -1 32 -33 IMP:h=1
31 100 -1 -1 33 -34 IMP:h=1
32 100 -1 -1 34 -35 IMP:h=1
33 100 -1 -1 35 -36 IMP:h=1
34 100 -1 -1 36 -37 IMP:h=1
35 100 -1 -1 37 -38 IMP:h=1
36 100 -1 -1 38 -39 IMP:h=1
37 100 -1 -1 39 -40 IMP:h=1
38 100 -1 -1 40 -41 IMP:h=1
```

39	100	-1	-1	41	-42	IMP:h=1
40	100	-1	-1	42	-43	IMP:h=1
41	100	-1	-1	43	-44	IMP:h=1
42	100	-1	-1	44	-45	IMP:h=1
43	100	-1	-1	45	-46	IMP:h=1
44	100	-1	-1	46	-47	IMP:h=1
45	100	-1	-1	47	-48	IMP:h=1
46	100	-1	-1	48	-49	IMP:h=1
47	100	-1	-1	49	-50	IMP:h=1
48	100	-1	-1	50	-51	IMP:h=1
49	100	-1	-1	51	-52	IMP:h=1
50	100	-1	-1	52	-53	IMP:h=1
51	100	-1	-1	53	-54	IMP:h=1
52	100	-1	-1	54	-55	IMP:h=1
53	100	-1	-1	55	-56	IMP:h=1
54	100	-1	-1	56	-57	IMP:h=1
55	100	-1	-1	57	-58	IMP:h=1
56	100	-1	-1	58	-59	IMP:h=1
57	100	-1	-1	59	-60	IMP:h=1
58	100	-1	-1	60	-61	IMP:h=1
59	100	-1	-1	61	-62	IMP:h=1
60	100	-1	-1	62	-63	IMP:h=1
61	100	-1	-1	63	-64	IMP:h=1
62	100	-1	-1	64	-65	IMP:h=1
63	100	-1	-1	65	-66	IMP:h=1
64	100	-1	-1	66	-67	IMP:h=1
65	100	-1	-1	67	-68	IMP:h=1
66	100	-1	-1	68	-69	IMP:h=1
67	100	-1	-1	69	-70	IMP:h=1
68	100	-1	-1	70	-71	IMP:h=1
69	100	-1	-1	71	-72	IMP:h=1
70	100	-1	-1	72	-73	IMP:h=1
71	100	-1	-1	73	-74	IMP:h=1
72	100	-1	-1	74	-75	IMP:h=1
73	100	-1	-1	75	-76	IMP:h=1
74	100	-1	-1	76	-77	IMP:h=1
75	100	-1	-1	77	-78	IMP:h=1
76	100	-1	-1	78	-79	IMP:h=1
77	100	-1	-1	79	-80	IMP:h=1
78	100	-1	-1	80	-81	IMP:h=1
79	100	-1	-1	81	-82	IMP:h=1
80	100	-1	-1	82	-83	IMP:h=1
81	100	-1	-1	83	-84	IMP:h=1
82	100	-1	-1	84	-85	IMP:h=1
83	100	-1	-1	85	-86	IMP:h=1
84	100	-1	-1	86	-87	IMP:h=1

85	100	-1	-1	87	-88	IMP:h=1
86	100	-1	-1	88	-89	IMP:h=1
87	100	-1	-1	89	-90	IMP:h=1
88	100	-1	-1	90	-91	IMP:h=1
89	100	-1	-1	91	-92	IMP:h=1
90	100	-1	-1	92	-93	IMP:h=1
91	100	-1	-1	93	-94	IMP:h=1
92	100	-1	-1	94	-95	IMP:h=1
93	100	-1	-1	95	-96	IMP:h=1
94	100	-1	-1	96	-97	IMP:h=1
95	100	-1	-1	97	-98	IMP:h=1
96	100	-1	-1	98	-99	IMP:h=1
97	100	-1	-1	99	-100	IMP:h=1
98	100	-1	-1	100	-101	IMP:h=1
99	100	-1	-1	101	-102	IMP:h=1
100	100	-1	-1	102	-103	IMP:h=1
101	100	-1	-1	103	-104	IMP:h=1
102	100	-1	-1	104	-105	IMP:h=1
103	100	-1	-1	105	-106	IMP:h=1
104	100	-1	-1	106	-107	IMP:h=1
105	100	-1	-1	107	-108	IMP:h=1
106	100	-1	-1	108	-109	IMP:h=1
107	100	-1	-1	109	-110	IMP:h=1
108	100	-1	-1	110	-111	IMP:h=1
109	100	-1	-1	111	-112	IMP:h=1
110	100	-1	-1	112	-113	IMP:h=1
111	100	-1	-1	113	-114	IMP:h=1
112	100	-1	-1	114	-115	IMP:h=1
113	100	-1	-1	115	-116	IMP:h=1
114	100	-1	-1	116	-117	IMP:h=1
115	100	-1	-1	117	-118	IMP:h=1
116	100	-1	-1	118	-119	IMP:h=1
117	100	-1	-1	119	-120	IMP:h=1
118	100	-1	-1	120	-121	IMP:h=1
119	100	-1	-1	121	-122	IMP:h=1
120	100	-1	-1	122	-123	IMP:h=1
121	100	-1	-1	123	-124	IMP:h=1
122	100	-1	-1	124	-125	IMP:h=1
123	100	-1	-1	125	-126	IMP:h=1
124	100	-1	-1	126	-127	IMP:h=1
125	100	-1	-1	127	-128	IMP:h=1
126	100	-1	-1	128	-129	IMP:h=1
127	100	-1	-1	129	-130	IMP:h=1
128	100	-1	-1	130	-131	IMP:h=1
129	100	-1	-1	131	-132	IMP:h=1
130	100	-1	-1	132	-133	IMP:h=1

131	100	-1	-1	133	-134	IMP:h=1
132	100	-1	-1	134	-135	IMP:h=1
133	100	-1	-1	135	-136	IMP:h=1
134	100	-1	-1	136	-137	IMP:h=1
135	100	-1	-1	137	-138	IMP:h=1
136	100	-1	-1	138	-139	IMP:h=1
137	100	-1	-1	139	-140	IMP:h=1
138	100	-1	-1	140	-141	IMP:h=1
139	100	-1	-1	141	-142	IMP:h=1
140	100	-1	-1	142	-143	IMP:h=1
141	100	-1	-1	143	-144	IMP:h=1
142	100	-1	-1	144	-145	IMP:h=1
143	100	-1	-1	145	-146	IMP:h=1
144	100	-1	-1	146	-147	IMP:h=1
145	100	-1	-1	147	-148	IMP:h=1
146	100	-1	-1	148	-149	IMP:h=1
147	100	-1	-1	149	-150	IMP:h=1
148	100	-1	-1	150	-151	IMP:h=1
149	100	-1	-1	151	-152	IMP:h=1
150	100	-1	-1	152	-153	IMP:h=1
151	100	-1	-1	153	-154	IMP:h=1
152	100	-1	-1	154	-155	IMP:h=1
153	100	-1	-1	155	-156	IMP:h=1
154	100	-1	-1	156	-157	IMP:h=1
155	100	-1	-1	157	-158	IMP:h=1
156	100	-1	-1	158	-159	IMP:h=1
157	100	-1	-1	159	-160	IMP:h=1
158	100	-1	-1	160	-161	IMP:h=1
159	100	-1	-1	161	-162	IMP:h=1
160	100	-1	-1	162	-163	IMP:h=1
161	100	-1	-1	163	-164	IMP:h=1
162	100	-1	-1	164	-165	IMP:h=1
163	100	-1	-1	165	-166	IMP:h=1
164	100	-1	-1	166	-167	IMP:h=1
165	100	-1	-1	167	-168	IMP:h=1
166	100	-1	-1	168	-169	IMP:h=1
167	100	-1	-1	169	-170	IMP:h=1
168	100	-1	-1	170	-171	IMP:h=1
169	100	-1	-1	171	-172	IMP:h=1
170	100	-1	-1	172	-173	IMP:h=1
171	100	-1	-1	173	-174	IMP:h=1
172	100	-1	-1	174	-175	IMP:h=1
173	100	-1	-1	175	-176	IMP:h=1
174	100	-1	-1	176	-177	IMP:h=1
175	100	-1	-1	177	-178	IMP:h=1
176	100	-1	-1	178	-179	IMP:h=1

177	100	-1	-1	179	-180	IMP:h=1
178	100	-1	-1	180	-181	IMP:h=1
179	100	-1	-1	181	-182	IMP:h=1
180	100	-1	-1	182	-183	IMP:h=1
181	100	-1	-1	183	-184	IMP:h=1
182	100	-1	-1	184	-185	IMP:h=1
183	100	-1	-1	185	-186	IMP:h=1
184	100	-1	-1	186	-187	IMP:h=1
185	100	-1	-1	187	-188	IMP:h=1
186	100	-1	-1	188	-189	IMP:h=1
187	100	-1	-1	189	-190	IMP:h=1
188	100	-1	-1	190	-191	IMP:h=1
189	100	-1	-1	191	-192	IMP:h=1
190	100	-1	-1	192	-193	IMP:h=1
191	100	-1	-1	193	-194	IMP:h=1
192	100	-1	-1	194	-195	IMP:h=1
193	100	-1	-1	195	-196	IMP:h=1
194	100	-1	-1	196	-197	IMP:h=1
195	100	-1	-1	197	-198	IMP:h=1
196	100	-1	-1	198	-199	IMP:h=1
197	100	-1	-1	199	-200	IMP:h=1
198	100	-1	-1	200	-201	IMP:h=1
199	100	-1	-1	201	-202	IMP:h=1
200	100	-1	-1	202	-203	IMP:h=1
201	100	-1	-1	203	-204	IMP:h=1
202	100	-1	-1	204	-205	IMP:h=1
203	100	-1	-1	205	-206	IMP:h=1
204	100	-1	-1	206	-207	IMP:h=1
205	100	-1	-1	207	-208	IMP:h=1
206	100	-1	-1	208	-209	IMP:h=1
207	100	-1	-1	209	-210	IMP:h=1
208	100	-1	-1	210	-211	IMP:h=1
209	100	-1	-1	211	-212	IMP:h=1
210	100	-1	-1	212	-213	IMP:h=1
211	100	-1	-1	213	-214	IMP:h=1
212	100	-1	-1	214	-215	IMP:h=1
213	100	-1	-1	215	-216	IMP:h=1
214	100	-1	-1	216	-217	IMP:h=1
215	100	-1	-1	217	-218	IMP:h=1
216	100	-1	-1	218	-219	IMP:h=1
217	100	-1	-1	219	-220	IMP:h=1
218	100	-1	-1	220	-221	IMP:h=1
219	100	-1	-1	221	-222	IMP:h=1
220	100	-1	-1	222	-223	IMP:h=1
221	100	-1	-1	223	-224	IMP:h=1
222	100	-1	-1	224	-225	IMP:h=1

223	100	-1	-1	225	-226	IMP:h=1
224	100	-1	-1	226	-227	IMP:h=1
225	100	-1	-1	227	-228	IMP:h=1
226	100	-1	-1	228	-229	IMP:h=1
227	100	-1	-1	229	-230	IMP:h=1
228	100	-1	-1	230	-231	IMP:h=1
229	100	-1	-1	231	-232	IMP:h=1
230	100	-1	-1	232	-233	IMP:h=1
231	100	-1	-1	233	-234	IMP:h=1
232	100	-1	-1	234	-235	IMP:h=1
233	100	-1	-1	235	-236	IMP:h=1
234	100	-1	-1	236	-237	IMP:h=1
235	100	-1	-1	237	-238	IMP:h=1
236	100	-1	-1	238	-239	IMP:h=1
237	100	-1	-1	239	-240	IMP:h=1
238	100	-1	-1	240	-241	IMP:h=1
239	100	-1	-1	241	-242	IMP:h=1
240	100	-1	-1	242	-243	IMP:h=1
241	100	-1	-1	243	-244	IMP:h=1
242	100	-1	-1	244	-245	IMP:h=1
243	100	-1	-1	245	-246	IMP:h=1
244	100	-1	-1	246	-247	IMP:h=1
245	100	-1	-1	247	-248	IMP:h=1
246	100	-1	-1	248	-249	IMP:h=1
247	100	-1	-1	249	-250	IMP:h=1
248	100	-1	-1	250	-251	IMP:h=1
249	100	-1	-1	251	-252	IMP:h=1
250	100	-1	-1	252	-253	IMP:h=1
251	100	-1	-1	253	-254	IMP:h=1
252	100	-1	-1	254	-255	IMP:h=1
253	100	-1	-1	255	-256	IMP:h=1
254	100	-1	-1	256	-257	IMP:h=1
255	100	-1	-1	257	-258	IMP:h=1
256	100	-1	-1	258	-259	IMP:h=1
257	100	-1	-1	259	-260	IMP:h=1
258	100	-1	-1	260	-261	IMP:h=1
259	100	-1	-1	261	-262	IMP:h=1
260	100	-1	-1	262	-263	IMP:h=1
1000	100	-1	-1			IMP:h=1
2000	0		1	-2		IMP:h=1
3000	0		2			IMP:h=0

c Surface card

1	RPP	0	30	-10	10	-10	10
2	RPP	-350	35	-30	30	-30	30
3	PX	0					

4	PX	0.05
5	PX	0.10
6	PX	0.15
7	PX	0.20
8	PX	0.25
9	PX	0.30
10	PX	0.35
11	PX	0.40
12	PX	0.45
13	PX	0.50
14	PX	0.55
15	PX	0.60
16	PX	0.65
17	PX	0.70
18	PX	0.75
19	PX	0.80
20	PX	0.85
21	PX	0.90
22	PX	0.95
23	PX	1.00
24	PX	1.05
25	PX	1.10
26	PX	1.15
27	PX	1.20
28	PX	1.25
29	PX	1.30
30	PX	1.35
31	PX	1.40
32	PX	1.45
33	PX	1.50
34	PX	1.55
35	PX	1.60
36	PX	1.65
37	PX	1.70
38	PX	1.75
39	PX	1.80
40	PX	1.85
41	PX	1.90
42	PX	1.95
43	PX	2.00
44	PX	2.05
45	PX	2.10
46	PX	2.15
47	PX	2.20
48	PX	2.25
49	PX	2.30

50	PX	2.35
51	PX	2.40
52	PX	2.45
53	PX	2.50
54	PX	2.55
55	PX	2.60
56	PX	2.65
57	PX	2.70
58	PX	2.75
59	PX	2.80
60	PX	2.85
61	PX	2.90
62	PX	2.95
63	PX	3.00
64	PX	3.05
65	PX	3.10
66	PX	3.15
67	PX	3.20
68	PX	3.25
69	PX	3.30
70	PX	3.35
71	PX	3.40
72	PX	3.45
73	PX	3.50
74	PX	3.55
75	PX	3.60
76	PX	3.65
77	PX	3.70
78	PX	3.75
79	PX	3.80
80	PX	3.85
81	PX	3.90
82	PX	3.95
83	PX	4.00
84	PX	4.05
85	PX	4.10
86	PX	4.15
87	PX	4.20
88	PX	4.25
89	PX	4.30
90	PX	4.35
91	PX	4.40
92	PX	4.45
93	PX	4.50
94	PX	4.55
95	PX	4.60

96	PX	4.65
97	PX	4.70
98	PX	4.75
99	PX	4.80
100	PX	4.85
101	PX	4.90
102	PX	4.95
103	PX	5.00
104	PX	5.05
105	PX	5.10
106	PX	5.15
107	PX	5.20
108	PX	5.25
109	PX	5.30
110	PX	5.35
111	PX	5.40
112	PX	5.45
113	PX	5.50
114	PX	5.55
115	PX	5.60
116	PX	5.65
117	PX	5.70
118	PX	5.75
119	PX	5.80
120	PX	5.85
121	PX	5.90
122	PX	5.95
123	PX	6.00
124	PX	6.05
125	PX	6.10
126	PX	6.15
127	PX	6.20
128	PX	6.25
129	PX	6.30
130	PX	6.35
131	PX	6.40
132	PX	6.45
133	PX	6.50
134	PX	6.55
135	PX	6.60
136	PX	6.65
137	PX	6.70
138	PX	6.75
139	PX	6.80
140	PX	6.85
141	PX	6.90

142	PX	6.95
143	PX	7.00
144	PX	7.05
145	PX	7.10
146	PX	7.15
147	PX	7.20
148	PX	7.25
149	PX	7.30
150	PX	7.35
151	PX	7.40
152	PX	7.45
153	PX	7.50
154	PX	7.55
155	PX	7.60
156	PX	7.65
157	PX	7.70
158	PX	7.75
159	PX	7.80
160	PX	7.85
161	PX	7.90
162	PX	7.95
163	PX	8.00
164	PX	8.05
165	PX	8.10
166	PX	8.15
167	PX	8.20
168	PX	8.25
169	PX	8.30
170	PX	8.35
171	PX	8.40
172	PX	8.45
173	PX	8.50
174	PX	8.55
175	PX	8.60
176	PX	8.65
177	PX	8.70
178	PX	8.75
179	PX	8.80
180	PX	8.85
181	PX	8.90
182	PX	8.95
183	PX	9.00
184	PX	9.05
185	PX	9.10
186	PX	9.15
187	PX	9.20

188	PX	9.25
189	PX	9.30
190	PX	9.35
191	PX	9.40
192	PX	9.45
193	PX	9.50
194	PX	9.55
195	PX	9.60
196	PX	9.65
197	PX	9.70
198	PX	9.75
199	PX	9.80
200	PX	9.85
201	PX	9.90
202	PX	9.95
203	PX	10.00
204	PX	10.05
205	PX	10.10
206	PX	10.15
207	PX	10.20
208	PX	10.25
209	PX	10.30
210	PX	10.35
211	PX	10.40
212	PX	10.45
213	PX	10.50
214	PX	10.55
215	PX	10.60
216	PX	10.65
217	PX	10.70
218	PX	10.75
219	PX	10.80
220	PX	10.85
221	PX	10.90
222	PX	10.95
223	PX	11.00
224	PX	11.05
225	PX	11.10
226	PX	11.15
227	PX	11.20
228	PX	11.25
229	PX	11.30
230	PX	11.35
231	PX	11.40
232	PX	11.45
233	PX	11.50

234 PX 11.55
 235 PX 11.60
 236 PX 11.65
 237 PX 11.70
 238 PX 11.75
 239 PX 11.80
 240 PX 11.85
 241 PX 11.90
 242 PX 11.95
 243 PX 12.00
 244 PX 12.05
 245 PX 12.10
 246 PX 12.15
 247 PX 12.20
 248 PX 12.25
 249 PX 12.30
 250 PX 12.35
 251 PX 12.40
 252 PX 12.45
 253 PX 12.50
 254 PX 12.55
 255 PX 12.60
 256 PX 12.65
 257 PX 12.70
 258 PX 12.75
 259 PX 12.80
 260 PX 12.85
 261 PX 12.90
 262 PX 12.95
 263 PX 13.00

c Data

MODE h

PHYS:h 121 0 -1 J 0 J 0 \$set max energy for protons to 121 MeV;
 else default

c Source

SDEF POS=-270.712275384282 0 0 ERG=121 PAR=h VEC=1 0 0 DIR=d1

SI1 -1 0.999976206 0.999980007 0.999983476 0.999986616
 0.999989425 0.999991903 0.999994051 0.999995869 0.999997356
 0.999998513 0.999999339 0.999999835 1

SP1 0 0.9999881032 0.0000019001 0.0000017349 0.0000015697
 0.0000014045 0.0000012393 0.0000010740 0.0000009088
 0.0000007436 0.0000005783 0.0000004131 0.0000002479
 0.0000000826

SB1 0 0 0.011685184 0.021142753 0.035622575 0.055775775
 0.080929884 0.108387301 0.133180894 0.148697298 0.148308942

0.127657301 0.086736332 0.030766766

c Tally

*f18:h 1
*f28:h 2
*f38:h 3
*f48:h 4
*f58:h 5
*f68:h 6
*f78:h 7
*f88:h 8
*f98:h 9
*f108:h 10
*f118:h 11
*f128:h 12
*f138:h 13
*f148:h 14
*f158:h 15
*f168:h 16
*f178:h 17
*f188:h 18
*f198:h 19
*f208:h 20
*f218:h 21
*f228:h 22
*f238:h 23
*f248:h 24
*f258:h 25
*f268:h 26
*f278:h 27
*f288:h 28
*f298:h 29
*f308:h 30
*f318:h 31
*f328:h 32
*f338:h 33
*f348:h 34
*f358:h 35
*f368:h 36
*f378:h 37
*f388:h 38
*f398:h 39
*f408:h 40
*f418:h 41
*f428:h 42
*f438:h 43
*f448:h 44

*f458:h 45
*f468:h 46
*f478:h 47
*f488:h 48
*f498:h 49
*f508:h 50
*f518:h 51
*f528:h 52
*f538:h 53
*f548:h 54
*f558:h 55
*f568:h 56
*f578:h 57
*f588:h 58
*f598:h 59
*f608:h 60
*f618:h 61
*f628:h 62
*f638:h 63
*f648:h 64
*f658:h 65
*f668:h 66
*f678:h 67
*f688:h 68
*f698:h 69
*f708:h 70
*f718:h 71
*f728:h 72
*f738:h 73
*f748:h 74
*f758:h 75
*f768:h 76
*f778:h 77
*f788:h 78
*f798:h 79
*f808:h 80
*f818:h 81
*f828:h 82
*f838:h 83
*f848:h 84
*f858:h 85
*f868:h 86
*f878:h 87
*f888:h 88
*f898:h 89
*f908:h 90

*f918:h 91
*f928:h 92
*f938:h 93
*f948:h 94
*f958:h 95
*f968:h 96
*f978:h 97
*f988:h 98
*f998:h 99
*f1008:h 100
*f1018:h 101
*f1028:h 102
*f1038:h 103
*f1048:h 104
*f1058:h 105
*f1068:h 106
*f1078:h 107
*f1088:h 108
*f1098:h 109
*f1108:h 110
*f1118:h 111
*f1128:h 112
*f1138:h 113
*f1148:h 114
*f1158:h 115
*f1168:h 116
*f1178:h 117
*f1188:h 118
*f1198:h 119
*f1208:h 120
*f1218:h 121
*f1228:h 122
*f1238:h 123
*f1248:h 124
*f1258:h 125
*f1268:h 126
*f1278:h 127
*f1288:h 128
*f1298:h 129
*f1308:h 130
*f1318:h 131
*f1328:h 132
*f1338:h 133
*f1348:h 134
*f1358:h 135
*f1368:h 136

*f1378:h 137
*f1388:h 138
*f1398:h 139
*f1408:h 140
*f1418:h 141
*f1428:h 142
*f1438:h 143
*f1448:h 144
*f1458:h 145
*f1468:h 146
*f1478:h 147
*f1488:h 148
*f1498:h 149
*f1508:h 150
*f1518:h 151
*f1528:h 152
*f1538:h 153
*f1548:h 154
*f1558:h 155
*f1568:h 156
*f1578:h 157
*f1588:h 158
*f1598:h 159
*f1608:h 160
*f1618:h 161
*f1628:h 162
*f1638:h 163
*f1648:h 164
*f1658:h 165
*f1668:h 166
*f1678:h 167
*f1688:h 168
*f1698:h 169
*f1708:h 170
*f1718:h 171
*f1728:h 172
*f1738:h 173
*f1748:h 174
*f1758:h 175
*f1768:h 176
*f1778:h 177
*f1788:h 178
*f1798:h 179
*f1808:h 180
*f1818:h 181
*f1828:h 182

*f1838:h 183
*f1848:h 184
*f1858:h 185
*f1868:h 186
*f1878:h 187
*f1888:h 188
*f1898:h 189
*f1908:h 190
*f1918:h 191
*f1928:h 192
*f1938:h 193
*f1948:h 194
*f1958:h 195
*f1968:h 196
*f1978:h 197
*f1988:h 198
*f1998:h 199
*f2008:h 200
*f2018:h 201
*f2028:h 202
*f2038:h 203
*f2048:h 204
*f2058:h 205
*f2068:h 206
*f2078:h 207
*f2088:h 208
*f2098:h 209
*f2108:h 210
*f2118:h 211
*f2128:h 212
*f2138:h 213
*f2148:h 214
*f2158:h 215
*f2168:h 216
*f2178:h 217
*f2188:h 218
*f2198:h 219
*f2208:h 220
*f2218:h 221
*f2228:h 222
*f2238:h 223
*f2248:h 224
*f2258:h 225
*f2268:h 226
*f2278:h 227
*f2288:h 228

*f2298:h 229
*f2308:h 230
*f2318:h 231
*f2328:h 232
*f2338:h 233
*f2348:h 234
*f2358:h 235
*f2368:h 236
*f2378:h 237
*f2388:h 238
*f2398:h 239
*f2408:h 240
*f2418:h 241
*f2428:h 242
*f2438:h 243
*f2448:h 244
*f2458:h 245
*f2468:h 246
*f2478:h 247
*f2488:h 248
*f2498:h 249
*f2508:h 250
*f2518:h 251
*f2528:h 252
*f2538:h 253
*f2548:h 254
*f2558:h 255
*f2568:h 256
*f2578:h 257
*f2588:h 258
*f2598:h 259
*f2608:h 260
c Material
M100 1000 2 8000 1
c Termination
NPS 500000

A.2 MCNP6 Beam 11 TMESH1 Tally Input at the Surface

```
Proton beam
c Cell card
1 1 -1 -1 IMP:h=1
2 0 1 -2 IMP:h=1
3 0 2 IMP:h=0

c Surface card
1 RPP 0 30 -10 10 -10 10
2 RPP -350 35 -30 30 -30 30

c Data
MODE h
PHYS:h 121 0 -1 J 0 J 0 $set max energy for protons to 121 MeV;
else default

c Source
SDEF POS=-270.712275384282 0 0 ERG=121 PAR=h VEC=0.9996257824
0.0179080359 -0.0206784283 DIR=d1
SI1 -1 0.999976206 0.999980007 0.999983476 0.999986616
0.999989425 0.999991903 0.999994051 0.999995869 0.999997356
0.999998513 0.999999339 0.999999835 1
SP1 0 0.9999881032 0.0000019001 0.0000017349 0.0000015697
0.0000014045 0.0000012393 0.0000010740 0.0000009088
0.0000007436 0.0000005783 0.0000004131 0.0000002479
0.0000000826
SB1 0 0 0.011685184 0.021142753 0.035622575 0.055775775
0.080929884 0.108387301 0.133180894 0.148697298 0.148308942
0.127657301 0.086736332 0.030766766

c Tally
TMESH
RMESH11:h TRAKS
CORA11 0 1i 0.5
CORB11 -10 199i 10
CORC11 -10 199i 10
ENDMD
c Material
M1 1000 2 8000 1
M2 6000 -0.000124 7000 -0.7552 8000 -0.231781 18000 -0.012827
c Termination
NPS 1000000
```

A.3 MCNP6 Beam 11 TMESH3 Tally Input at the Surface

```
Proton beam
c Cell card
1 1 -1 -1 IMP:h=1
2 0 1 -2 IMP:h=1
3 0 2 IMP:h=0

c Surface card
1 RPP 0 30 -10 10 -10 10 $This is greater than width/length
12.3/13.5
2 RPP -350 35 -30 30 -30 30

c Data
MODE h
PHYS:h 121 0 -1 J 0 J 0 $set max energy for protons to 121 MeV;
else default
c Source
SDEF POS=-270.712275384282 0 0 ERG=121 PAR=h VEC=0.9996257824
0.0179080359 -0.0206784283 DIR=d1
SI1 -1 0.999976206 0.999980007 0.999983476 0.999986616
0.999989425 0.999991903 0.999994051 0.999995869 0.999997356
0.999998513 0.999999339 0.999999835 1
SP1 0 0.9999881032 0.0000019001 0.0000017349 0.0000015697
0.0000014045 0.0000012393 0.0000010740 0.0000009088
0.0000007436 0.0000005783 0.0000004131 0.0000002479
0.0000000826
SB1 0 0 0.011685184 0.021142753 0.035622575 0.055775775
0.080929884 0.108387301 0.133180894 0.148697298 0.148308942
0.127657301 0.086736332 0.030766766

c Tally
TMESH
RMESH13 TOTAL
CORAI3 0 1i 0.5
CORB13 -10 199i 10
CORC13 -10 199i 10
ENDMD
c Material
M1 1000 2 8000 1
c Termination
NPS 1000000
```

APPENDIX B: MATLAB ANALYSIS FILES

B.1 TMESH Tally Code: MdataReader

```
function [out1, out2]=MdataReader(fname)
a=ReadMData(fname);
a=a.Mesh;
a=a{1};
out1=a.Tally;
out2 = a.Error;
end
```

B.2 TMESH Tally Code: ReadMData

```
function mdata = ReadMData(filename)
% ReadMData(filename) Returns a structure containing the tally information
% from an MCNPX mdata mesh tally file (in binary, not ASCII, format)
% specified by filename. Calling the function without a filename will
% show a file browser. Much of this function is based on the FORTRAN
% source code of gridconv, but it does not duplicate all of that tool's
% functionality.

% Daniel Warren
% Particle Therapy Cancer Research Institute
% University of Oxford
%
% This work is licenced under the Creative Commons Attribution-NonCommercial
% 3.0 Unported License. To view a copy of this licence, visit
% http://creativecommons.org/licenses/by-nc/3.0/ or send a letter to
% Creative Commons, 171 Second Street, Suite 300, San Francisco, California
% 94105, USA.

if ~exist('filename','var')
    [fn pn] = uigetfile('*','Select mdata file');
    filename = [pn fn];
end

h=waitbar(0,'Stage 0 - indexing mdata file');

hfd = ReadFORTRANBinary(filename);

mdata.ProblemTitle = char(ReadRecord(hfd))';
hfd = NextRecord(hfd);
mdata.NumberOfMeshes = typecast(ReadRecord(hfd,1:4),'uint32');
mdata.CodeVersion = [char(ReadRecord(hfd,5:12))'
char(ReadRecord(hfd,13:17))'];
mdata.TimeOfRun = char(ReadRecord(hfd,18:45))';
mdata.NumberOfParticles = typecast(ReadRecord(hfd,46:49),'uint32');
hfd = NextRecord(hfd);
hfd = NextRecord(hfd);
for i=1:mdata.NumberOfMeshes
```

```

mdata.Mesh{i}.GridType=typecast (ReadRecord (hfd,1:4), 'uint32');
mdata.Mesh{i}.igpt=typecast (ReadRecord (hfd,5:8), 'uint32');
mdata.Mesh{i}.SizeOfDimension1=typecast (ReadRecord (hfd,9:12), 'uint32')-1;
mdata.Mesh{i}.SizeOfDimension2=typecast (ReadRecord (hfd,13:16), 'uint32')-
1;
mdata.Mesh{i}.SizeOfDimension3=typecast (ReadRecord (hfd,17:20), 'uint32')-
1;
mdata.Mesh{i}.mxgv=typecast (ReadRecord (hfd,21:24), 'uint32');
mdata.Mesh{i}.mxgc=typecast (ReadRecord (hfd,25:28), 'uint32');
mdata.Mesh{i}.nugd=typecast (ReadRecord (hfd,29:32), 'uint32');
mdata.Mesh{i}.mxgt=typecast (ReadRecord (hfd,33:36), 'uint32');
hfd=NextRecord (hfd);
mdata.Mesh{i}.EnergyLow = typecast (ReadRecord (hfd,1:8), 'double');
mdata.Mesh{i}.EnergyHigh = typecast (ReadRecord (hfd,9:16), 'double');
hfd=NextRecord (hfd);
hfd=NextRecord (hfd);
hfd=NextRecord (hfd);

end

for ig=1:mdata.NumberOfMeshes
nt=mdata.Mesh{ig}.GridType/10;

gdx = zeros ((mdata.Mesh{ig}.SizeOfDimension1+1),1, 'double');
for i = 1:(mdata.Mesh{ig}.SizeOfDimension1+1)
gdx(i) = typecast (ReadRecord (hfd,1+(i-1)*8:8*i), 'double');
end
mdata.Mesh{ig}.Dimension1Bins = gdx(1:mdata.Mesh{ig}.SizeOfDimension1+1);
hfd = NextRecord (hfd);

gdy = zeros (mdata.Mesh{ig}.SizeOfDimension2+1,1, 'double');
for i = 1:(mdata.Mesh{ig}.SizeOfDimension2+1)
gdy(i) = typecast (ReadRecord (hfd,1+(i-1)*8:8*i), 'double');
end
mdata.Mesh{ig}.Dimension2Bins = gdy(1:mdata.Mesh{ig}.SizeOfDimension2+1);
hfd = NextRecord (hfd);

gdz = zeros (mdata.Mesh{ig}.SizeOfDimension3+1,1, 'double');
for i = 1:(mdata.Mesh{ig}.SizeOfDimension3+1)
gdz(i) = typecast (ReadRecord (hfd,1+(i-1)*8:8*i), 'double');
end
mdata.Mesh{ig}.Dimension3Bins = gdz(1:mdata.Mesh{ig}.SizeOfDimension3+1);
hfd = NextRecord (hfd);

mzmax =
(mdata.Mesh{ig}.SizeOfDimension3) * (mdata.Mesh{ig}.SizeOfDimension1) * (mdata.Me
sh{ig}.SizeOfDimension2+1) + (mdata.Mesh{ig}.SizeOfDimension2) * (mdata.Mesh{ig}.
SizeOfDimension1);

gdata=zeros (mdata.Mesh{ig}.mxgc+mzmax+mdata.Mesh{ig}.SizeOfDimension1,1, 'doub
le');

if nt == 3

```



```

        mdata.Mesh{ig}.SizeOfDimension2 =
(mdata.Mesh{ig}.SizeOfDimension2+1);
    end

    if nt ~= 1
        mdata.Mesh{ig}.SizeOfDimension3 =
(mdata.Mesh{ig}.SizeOfDimension3+1);
    end

    for iv=1:mdata.Mesh{ig}.mxgv
        for k=1:mdata.Mesh{ig}.SizeOfDimension3

waitbar((1/3)*double(k)/double(mdata.Mesh{ig}.SizeOfDimension3),h,'Stage 1 -
reading tally');
            for j=1:mdata.Mesh{ig}.SizeOfDimension2
                mz=(k-1)*((mdata.Mesh{ig}.SizeOfDimension1+1)-
1)*mdata.Mesh{ig}.SizeOfDimension2+(j-1)*(mdata.Mesh{ig}.SizeOfDimension1);
                gdata(mz+1:mz+mdata.Mesh{ig}.SizeOfDimension1) =
typecast(ReadRecord(hfd,1:8*mdata.Mesh{ig}.SizeOfDimension1),'double');
                hfd = NextRecord(hfd);
            end

        end

        for k=1:mdata.Mesh{ig}.SizeOfDimension3

waitbar((1/3)+(1/3)*double(k)/double(mdata.Mesh{ig}.SizeOfDimension3),h,'Stag
e 2 - reading variance');

            for j=1:mdata.Mesh{ig}.SizeOfDimension2
                mz=(k-1)*((mdata.Mesh{ig}.SizeOfDimension1+1)-
1)*mdata.Mesh{ig}.SizeOfDimension2+(j-
1)*((mdata.Mesh{ig}.SizeOfDimension1+1)-1);

gdata(mz+mdata.Mesh{ig}.mxgc+1:mz+mdata.Mesh{ig}.mxgc+(mdata.Mesh{ig}.SizeOfD
imension1+1)-1) =
typecast(ReadRecord(hfd,1:8*((mdata.Mesh{ig}.SizeOfDimension1+1)-
1)),'double');

                hfd = NextRecord(hfd);

            end

        end

        fpi=1/double(mdata.NumberOfParticles);

        for k=1:mdata.Mesh{ig}.SizeOfDimension3

waitbar((2/3)+(1/3)*double(k)/double(mdata.Mesh{ig}.SizeOfDimension3),h,'Stag
e 3 - scaling data');

            for j=1:mdata.Mesh{ig}.SizeOfDimension2

```



```

% This work is licenced under the Creative Commons Attribution-NonCommercial
% 3.0 Unported License. To view a copy of this licence, visit
% http://creativecommons.org/licenses/by-nc/3.0/ or send a letter to
% Creative Commons, 171 Second Street, Suite 300, San Francisco, California
% 94105, USA.

```

```

h=waitbar(0,'Indexing FORTRAN unformatted data file...');
fid=fopen(filename,'r','n');
i = 0;
fseek(fid,0,'eof');
filesize = ftell(fid);
maxrecords = ceil(filesize/8);
frewind(fid);

```

```

RecordLengths = zeros(maxrecords,1,'uint32');
RecordStarts = zeros(maxrecords,1,'uint32');
RecordData = cell(maxrecords,1);

```

```

endoffile=0;
while ~endoffile
    waitbar(ftell(fid)/filesize,h,'Indexing FORTRAN unformatted data
file...');
    i=i+1;
    RecordLength = fread(fid,1,'*uint32');
    if ~isempty(RecordLength)
        RecordLengths(i) = RecordLength;
        RecordStarts(i) = ftell(fid);
        RecordData{i} = fread(fid,RecordLengths(i),'*ubit8');
        fseek(fid,4,'cof'); % skip record footer
    else
        endoffile = 1;
    end
end

```

```

fclose(fid);

```

```

IndexOut.RecordLengths = RecordLengths(1:i);
IndexOut.RecordStarts = RecordStarts(1:i);
IndexOut.RecordData = RecordData(1:i);
IndexOut.FileName = filename;
IndexOut.RecordCounter = 1;
close(h);

```

B.4 TMESH Tally Code: NextRecord

```

function IndexOut = NextRecord(IndexIn)
% NextRecord(IndexIn) Increments the record counter in the indexed FORTRAN
% unformatted data file stored in the structure IndexIn.

% Daniel Warren
% Particle Therapy Cancer Research Institute
% University of Oxford
%
% This work is licenced under the Creative Commons Attribution-NonCommercial

```

```

% 3.0 Unported License. To view a copy of this licence, visit
% http://creativecommons.org/licenses/by-nc/3.0/ or send a letter to
% Creative Commons, 171 Second Street, Suite 300, San Francisco, California
% 94105, USA.

```

```

IndexIn.RecordCounter = IndexIn.RecordCounter+1;
IndexOut=IndexIn;

```

B.5 TMESH Tally Code: ReadRecord

```

function [ OutData ] = ReadRecord( IndexIn, Range )
% ReadRecord(IndexIn, Range) Returns the content of the current record in
% the indexed FORTRAN unformatted data file stored in the structure
% IndexIn. The bytes returned are represented as uint8. A subset of the
% bytes can be selected by the optional parameter Range.
%
% eg.
%     a = ReadRecord(Index,1:8);
%     b = typecast(a,'double');
% a is a uint8 representation of the first 8 bytes of the current record
% in Index. b is the double precision floating point value corresponding
% to those bytes.
%
% Daniel Warren
% Particle Therapy Cancer Research Institute
% University of Oxford
%
% This work is licenced under the Creative Commons Attribution-NonCommercial
% 3.0 Unported License. To view a copy of this licence, visit
% http://creativecommons.org/licenses/by-nc/3.0/ or send a letter to
% Creative Commons, 171 Second Street, Suite 300, San Francisco, California
% 94105, USA.
%
if ~exist('Range','var')
OutData = IndexIn.RecordData{IndexIn.RecordCounter};
else
    OutData = IndexIn.RecordData{IndexIn.RecordCounter}(Range);
end

```

B.6 Gamma Analysis Code: CalcGamma

```

function gamma = CalcGamma(varargin)
% CalcGamma computes 1-D, 2-D, or 3-D global or absolute gamma between two
% datasets (reference and target) given a defined coordinate space. The
% datasets must have the same number of dimensions, although they can be
% different sizes. Gamma will be computed for each target dose point by
% shifting the reference image (using linear interpolation) and determining
% the minimum Gamma index across all shifts.
%
% This function optionally uses the Parallel Computing Toolbox GPU interp
% functions to increase computation speed. A try-catch statement is used
% to test for GPU support. In addition, for memory management, the

```

```

% meshgrid and data arrays are converted to single precision during
% interpolation. This function calls Event() to log execution status, if
% available.
%
% For more information on the Gamma evaluation function, see D. A. Low et
% al., "A technique for the quantitative evaluation of dose distributions",
% Med Phys. 1998 May; 25(5): 656-61.
%
% The following variables are required for proper execution:
%   varargin{1}: structure containing the reference data, where the field
%     start is an array containing the coordinates along each dimension
%     of the first voxel, width is an array containing the width of each
%     voxel along each dimension, and data is an n-dimensional array
%   varargin{2}: structure containing the target data, where the field
%     start is an array containing the coordinates along each dimension
%     of the first voxel, width is an array containing the width of each
%     voxel along each dimension, and data is an n-dimensional array
%   varargin{3}: Gamma absolute criterion percentage
%   varargin{4}: Gamma Distance To Agreement (DTA) criterion, in the same
%     units as the reference and target width structure fields
%   varargin{5:end} (optional): additional parameters preceded by option
%     flags. The available options are 'local', 'refval', 'restrict',
%     'res', and 'limit'.
%
% The following options can be passed to this argument as name/value pairs:
%   local: boolean, indicates whether to perform a local (1) or global (0)
%     Gamma computation. If not present, the function will assume a
%     global Gamma computation.
%   refval: reference value for the global absolute criterion. Is used with
%     the percentage from varargin{3} to compute absolute value. If not
%     present, the maximum value in the reference data is used.
%   restrict: restricted search flag. If 1, only the gamma values along the
%     X/Y/Z axes are computed during 3D computation. If 0 or not provided,
%     the entire rectangular search space is computed.
%   res: DTA resolution factor. The number of distance steps equal the
%     resolution factor multiplied by the limit. If not provided, the
%     factor is 100 for 1D/2D and 20 for 3D calculations.
%   limit: The DTA limit. This number determines how far the function will
%     search in the distance axes when computing Gamma. This also
%     therefore specifies the maximum "real" Gamma Index value.
%   cpu: boolean, set to 1 to force CPU computation.
%
% The following variables are returned upon successful completion:
%   gamma: array of the same dimensions as varargin{2}.data containing the
%     computed gamma values
%
% Below is an example of how the function is used:
%
%   reference.start = [-10 -10]; % mm
%   reference.width = [0.1 0.1]; % mm
%   reference.data = rand(200);
%
%   target.start = [-10 -10]; % mm
%   target.width = [0.1 0.1]; % mm
%   target.data = rand(200);
%
%   percent = 3;

```

```

%   dta = 0.5; % mm
%   local = 0; % Perform global gamma
%
%   gamma = CalcGamma(reference, target, percent, dta, 'local', local);
%
% Author: Mark Geurts, mark.w.geurts@gmail.com
% Copyright (C) 2014 University of Wisconsin Board of Regents
%
% This program is free software: you can redistribute it and/or modify it
% under the terms of the GNU General Public License as published by the
% Free Software Foundation, either version 3 of the License, or (at your
% option) any later version.
%
% This program is distributed in the hope that it will be useful, but
% WITHOUT ANY WARRANTY; without even the implied warranty of
% MERCHANTABILITY or FITNESS FOR A PARTICULAR PURPOSE. See the GNU General
% Public License for more details.
%
% You should have received a copy of the GNU General Public License along
% with this program. If not, see http://www.gnu.org/licenses/.

%% Validate Inputs
% Verify at least four input arguments are provided
if nargin < 4

    % If not, throw an error and stop execution
    if exist('Event', 'file') == 2
        Event('Too few input argumenst passed to CalcGamma', 'ERROR');
    else
        error('Too few input argumenst passed to CalcGamma');
    end
end

% Check if the reference structure contains width, start, and data fields,
% and if the size of the width and start vectors are equal
if ~isfield(varargin{1}, 'width') || ~isfield(varargin{1}, 'start') || ...
    ~isfield(varargin{1}, 'data') || ~isequal(size(varargin{1}.width),
    ...
        size(varargin{1}.start))

    % If not, throw an error and stop execution
    if exist('Event', 'file') == 2
        Event(['Incorrect reference data format. Must contain width, ', ...
            'start, and data fields and be of equal dimensions'], 'ERROR');
    else
        error(['Incorrect reference data format. Must contain width, ', ...
            'start, and data fields and be of equal dimensions']);
    end
end

% Check if the target structure contains width, start, and data fields,
% and if the size of the width and start vectors are equal
elseif ~isfield(varargin{2}, 'width') || ~isfield(varargin{2}, 'start') ||
    ...
        ~isfield(varargin{2}, 'data') || ~isequal(size(varargin{2}.width),
    ...
        size(varargin{2}.start))

```

```

% If not, throw an error and stop execution
if exist('Event', 'file') == 2
    Event(['Incorrect target data format. Must contain width, ', ...
          'start, and data fields and be of equal dimensions'], 'ERROR');
else
    error(['Incorrect target data format. Must contain width, ', ...
          'start, and data fields and be of equal dimensions']);
end

% Check if the reference and target data arrays are the same number of
% dimensions. Calculating the gamma from a lower dimensional dataset to a
% higher dimensional reference is currently not supported
elseif ~isequal(size(size(varargin{1}.data)), size(size(varargin{2}.data)))

    % If not, throw an error and stop execution
    if exist('Event', 'file') == 2
        Event(['The fixed and target data arrays must be of the same', ...
              ' dimensions'], 'ERROR');
    else
        error(['The fixed and target data arrays must be of the same', ...
              ' dimensions']);
    end
end

end

% Log validation completed
if exist('Event', 'file') == 2
    Event('Data validation completed, beginning Gamma computation');
    tic;
end

%% Declare default options
% local indicates whether to perform a local (1) or global (0) Gamma
% computation. If not present, the function will assume a global Gamma
% computation.
local = 0;

% refval is the reference value for the global absolute criterion. Is used
% with the percentage from varargin{3} to compute absolute value. If not
% present, the maximum value in the reference data is used.
refval = max(max(max(varargin{1}.data)));

% restricted search flag. If 1, only the gamma values along the X/Y/Z axes
% are computed during 3D computation. If 0 or not provided, the entire
% rectangular search space is computed.
restrict = 0;

% The resolution parameter determines the number of steps (relative to
% the distance to agreement) that each reference voxel will be
% interpolated to and gamma calculated. A value of 5 with a DTA of 3
% mm means that gamma will be calculated at intervals of 3/5 = 0.6 mm.
% Different resolutions can be set for different dimensions of data.
if size(varargin{2}.width,2) == 1

    % Set 1-D resolution

```

```

    res = 100;

elseif size(varargin{2}.width,2) == 2

    % Set 2-D resolution
    res = 50;

elseif size(varargin{2}.width,2) == 3

    % Set 3-D resolution
    res = 20;

end

% The search limit parameter determines how far the function will search in
% the distance axes when computing Gamma. This also therefore specifies
% the maximum believable Gamma Index value. Typically this value is 2.
% This should always be set to an integer.
limit = 2;

%% Search for provided options
% Load data structure from varargin
for i = 5:nargin

    % If the local option is set
    if strcmp(varargin{i}, 'local')
        local = varargin{i+1};

    % If the refval option is set
    elseif strcmp(varargin{i}, 'refval')
        refval = varargin{i+1};

    % If the restrict option is set
    elseif strcmp(varargin{i}, 'restrict')
        restrict = varargin{i+1};

    % If the res option is set
    elseif strcmp(varargin{i}, 'res')
        res = varargin{i+1};

    % If the limit option is set
    elseif strcmp(varargin{i}, 'limit')
        limit = varargin{i+1};

    % If the cpu option is set
    elseif strcmp(varargin{i}, 'cpu')
        cpu = varargin{i+1};
    end
end

%% Log options
% If Event reporting is enabled
if exist('Event', 'file') == 2

```



```

% Log local
if local == 1
    Event('Gamma calculation set to local');
else
    Event('Gamma calculation assumed to global');
end

% Log refval
Event(sprintf('Reference value set to %g', refval));

% Log restrict
if restrict == 1
    Event('Restricted search enabled');
else
    Event('Restricted search disabled');
end

% Log res
Event(sprintf('Resolution set to %g', res));

% Log limit
Event(sprintf('DTA limit set to %g', limit));
end

%% Compute mesh grids
% If the reference dataset is 1-D
if size(varargin{1}.width,2) == 1

    % Log event
    if exist('Event', 'file') == 2
        Event('Reference dataset is 1-D');
    end

    % Check if the data is in rows or columns (this is only needed for 1-D)
    if size(varargin{1}.data,1) > size(varargin{1}.data,2)

        % If in rows, transpose
        varargin{1}.data = varargin{1}.data';
    end

    % Compute the reference X coordinates using the start and width values
    refX =
single(varargin{1}.start(1):varargin{1}.width(1):varargin{1}.start(1) ...
    + varargin{1}.width(1) * (size(varargin{1}.data,2) - 1));

% Otherwise, if the reference dataset is 2-D
elseif size(varargin{1}.width,2) == 2

    % Log event
    if exist('Event', 'file') == 2
        Event('Reference dataset is 2-D');
    end

    % Compute X and Y meshgrids for the reference dataset positions using

```

```

% the start and width values
[refX, refY] = meshgrid(single(varargin{1}.start(1):varargin{1}.width(1):
...
    varargin{1}.start(1) + varargin{1}.width(1) * ...
    (size(varargin{1}.data,1) - 1)), single(varargin{1}.start(2): ...
    varargin{1}.width(2):varargin{1}.start(2)...
    + varargin{1}.width(2) * (size(varargin{1}.data,2) - 1));

% Otherwise, if the reference dataset is 3-D
elseif size(varargin{1}.width,2) == 3

% Log event
if exist('Event', 'file') == 2
    Event('Reference dataset is 3-D');
end

% Compute X, Y, and Z meshgrids for the reference dataset positions
% using the start and width values, permuting X/Y
[refX, refY, refZ] = meshgrid(single(varargin{1}.start(2): ...
    varargin{1}.width(2):varargin{1}.start(2) + varargin{1}.width(2) *
...
    (size(varargin{1}.data,2) - 1)), single(varargin{1}.start(1): ...
    varargin{1}.width(1):varargin{1}.start(1) + varargin{1}.width(1)...
    * (size(varargin{1}.data,1) - 1)), single(varargin{1}.start(3):...
    varargin{1}.width(3):varargin{1}.start(3) + varargin{1}.width(3)...
    * (size(varargin{1}.data,3) - 1));

% Otherwise, if the reference data is of higher dimension
else

% Throw an error and stop execution
if exist('Event', 'file') == 2
    Event('The fixed data structure contains too many dimensions', ...
        'ERROR');
else
    error('The fixed data structure contains too many dimensions');
end
end

% If the target dataset is 1-D
if size(varargin{2}.width,2) == 1

% Log event
if exist('Event', 'file') == 2
    Event('Target dataset is 1-D');
end

% Check if the data is in rows or columns (this is only needed for 1-D)
if size(varargin{2}.data,1) > size(varargin{2}.data,2)

% If in rows, transpose
varargin{2}.data = varargin{2}.data';
end

% Compute the target X coordinates using the start and width values

```

```

    tarX =
single(varargin{2}.start(1):varargin{2}.width(1):varargin{2}.start(1) ...
    + varargin{2}.width(1) * (size(varargin{2}.data,2) - 1));

% Otherwise, if the target dataset is 2-D
elseif size(varargin{2}.width,2) == 2

    % Log event
    if exist('Event', 'file') == 2
        Event('Target dataset is 2-D');
    end

    % Compute X and Y meshgrids for the target dataset positions using the
    % start and width values
    [tarX, tarY] = meshgrid(single(varargin{2}.start(1):varargin{2}.width(1):
...
        varargin{2}.start(1) + varargin{2}.width(1) * ...
        (size(varargin{2}.data,1) - 1)), single(varargin{2}.start(2): ...
        varargin{2}.width(2):varargin{2}.start(2)...
        + varargin{2}.width(2) * (size(varargin{2}.data,2) - 1));

% Otherwise, if the target dataset is 3-D
elseif size(varargin{2}.width,2) == 3

    % Log event
    if exist('Event', 'file') == 2
        Event('Target dataset is 3-D');
    end

    % Compute X, Y, and Z meshgrids for the target dataset positions using
    % the start and width values, permuting X/Y
    [tarX, tarY, tarZ] = meshgrid(single(varargin{2}.start(2):...
        varargin{2}.width(2):varargin{2}.start(2) + varargin{2}.width(2) *
...
        (size(varargin{2}.data,2) - 1)), single(varargin{2}.start(1): ...
        varargin{2}.width(1):varargin{2}.start(1) + varargin{2}.width(1) ...
        * (size(varargin{2}.data,1) - 1)), single(varargin{2}.start(3):...
        varargin{2}.width(3):varargin{2}.start(3) + varargin{2}.width(3) ...
        * (size(varargin{2}.data,3) - 1));

end

%% Initialize variables
% Generate an initial gamma volume with values of 2^2 (this is the maximum
% reliable value of gamma, see description of limit above). Note that
% gamma-squared is stored during computation; sqrt is computed at the end.
gamma = ones(size(varargin{2}.data)) * (limit ^ 2);

% Log number of gamma calculations (for status updates on 3D calcs)
if restrict == 1

    % Compute number of restricted search calcs
    num = res * (limit * 2) * size(varargin{2}.width, 2);
else

```

```

    % Compute total number of calcs
    num = res * (limit * 2) ^ size(varargin{2}.width, 2);
end

% num is the number of iterations, num * numel the total number of
% interpolations being performed
if exist('Event', 'file') == 2
    Event(sprintf('Number of gamma calculations = %g', num * numel(gamma)));
end

% Initialize counter (for progress indicator)
n = 0;

%% Begin computation
% Start try-catch block to safely test for CUDA functionality
try
    % If the cpu option is set, throw an error to force CPU computation
    if exist('cpu', 'var') == 1 && cpu == 1
        error('Reverting to CPU computation');
    end

    % Clear and initialize GPU memory.  If CUDA is not enabled, or if the
    % Parallel Computing Toolbox is not installed, this will error, and the
    % function will automatically revert to CPU computation via the catch
    % statement
    gpuDevice(1);

    % Start a for loop to interpolate the dose array along the x-direction.
    % Note to support parfor loops indices must be integers, so x varies
    % from -2 to +2 multiplied by the number of interpolation steps.
    % Effectively, this evaluates gamma from -2 * DTA to +2 * DTA.
    for x = -limit*res:limit*res

        % i is the x axis step value
        i = x/res * varargin{4};

        % Initialize j and k as zero (they will be updated if the data is
        % of higher dimension)
        j = 0;
        k = 0;

        % If the data contains a second dimension
        if size(varargin{1}.width,2) > 1

            % Start a for loop to interpolate the dose array along the
            % y-direction.  Note to support parfor loops indices must be
            % integers, so y varies from -2 to +2 multiplied by the number
            % of interpolation steps.  Effectively, this evaluates gamma
            % from -2 * DTA to +2 * DTA.
            for y = -limit*res:limit*res

                % j is the y axis step value
                j = y/res * varargin{4};

                % Initialize k as zero (it will be updated if the data is

```

```

% of higher dimension)
k = 0;

% If the data contains a third dimension
if size(varargin{1}.width, 2) > 2

    % Start a for loop to interpolate the dose array along
    % the z-direction. Note to support parfor loops
    % indices must be integers, so z varies from -2 to +2
    % multiplied by the number of interpolation steps.
    % Effectively, this evaluates gamma from -2 * DTA to
    % +2 * DTA.
    for z = -limit*res:limit*res

        % k is the z axis step value
        k = z/res * varargin{4};

        % Check restricted search flag
        if restrict == 0 || sum(abs([x y z]) > 0) == 1

            % Run GPU interp3 function to compute the
            % values at the specified target coordinate
            interp = gather(interp3(gpuArray(refX),
                gpuArray(refY), ...
                gpuArray(refZ),
                gpuArray(single(varargin{1}.data)), ...
                gpuArray(tarX + i), gpuArray(tarY + j), ...
                gpuArray(tarZ + k), 'linear', 0));

            % Update the gamma array by returning the minimum
            % of the existing value or the new value
            gamma = min(gamma, GammaEquation(interp, ...
                varargin{2}.data, i, j, k, varargin{3},
                varargin{4}, ...
                refval, local));

            % Update counter
            n = n + 1;

            % If counter is at an even %, display progress
            if mod((n-1)/num, 0.01) > 0.005 && ...
                mod(n/num, 0.01) < 0.005
                fprintf('%0.1f%%\n', n/num*100);
            end
        end
    end
end

% Otherwise, the data is 2-D
else

    % Run GPU interp2 function to compute the reference
    % values at the specified target coordinate points

```

```

        interp = gather(interp2(gpuArray(refX), gpuArray(refY),
...
        gpuArray(single(varargin{1}.data)), gpuArray(tarX +
i), ...
        gpuArray(tarY + j), 'linear', 0));

        % Update the gamma array by returning the minimum
        % of the existing value or the new value
        gamma = min(gamma, GammaEquation(interp,
varargin{2}.data, ...
        i, j, k, varargin{3}, varargin{4}, ...
        refval, local));
    end
end

% Otherwise, the data is 1-D
else

    % Run GPU interp function to compute the reference values at
    % the specified target coordinate points
    interp = gather(interp1(gpuArray(refX), ...
        gpuArray(single(varargin{1}.data)), gpuArray(tarX + i), ...
        'linear', 0));

    % Update the gamma array by returning the minimum of the
    % existing value or the new value
    gamma = min(gamma, GammaEquation(interp, varargin{2}.data, ...
        i, j, k, varargin{3}, varargin{4}, ...
        refval, local));
end
end

% If GPU fails, revert to CPU computation
catch

    % Log GPU failure (if cpu flag is not set)
    if exist('Event', 'file') == 2 && exist('cpu', 'var') ~= 1
        Event('GPU failed, reverting to CPU method', 'WARN');
    end

    % Start a for loop to interpolate the dose array along the x-direction.
    % Note to support parfor loops indices must be integers, so x varies
    % from -2 to +2 multiplied by the number of interpolation steps.
    % Effectively, this evaluates gamma from -2 * DTA to +2 * DTA.
    for x = -limit*res:limit*res

        % i is the x axis step value
        i = x/res * varargin{4};

        % Initialize j and k as zero (they will be updated if the data is
        % of higher dimension)
        j = 0;
        k = 0;

        % If the data contains a second dimension

```

```

if size(varargin{1}.width, 2) > 1

    % Start a for loop to interpolate the dose array along the
    % y-direction. Note to support parfor loops indices must be
    % integers, so y varies from -2 to +2 multiplied by the number
    % of interpolation steps. Effectively, this evaluates gamma
    % from -2 * DTA to +2 * DTA.
    for y = -limit*res:limit*res

        % j is the y axis step value
        j = y/res * varargin{4};

        % Initialize k as zero (it will be updated if the data is
        % of higher dimension)
        k = 0;

        % If the data contains a third dimension
        if size(varargin{1}.width, 2) > 2

            % Start a for loop to interpolate the dose array along
            % the z-direction. Note to support parfor loops
            % indices must be integers, so z varies from -2 to +2
            % multiplied by the number of interpolation steps.
            % Effectively, this evaluates gamma from -2 * DTA to
            % +2 * DTA.
            for z = -limit*res:limit*res

                % k is the z axis step value
                k = z/res * varargin{4};

                % Check restricted search flag
                if restrict == 0 || sum(abs([x y z]) > 0) == 1

                    % Run CPU interp3 function to compute the
                    % values at the specified target coordinate
                    interp = interp3(refX, refY, refZ, ...
                        single(varargin{1}.data), tarX + i, ...
                        tarY + j, tarZ + k, '*linear', 0);

                    % Update the gamma array by returning the minimum
                    % of the existing value or the new value
                    gamma = min(gamma, GammaEquation(interp, ...
                        varargin{2}.data, i, j, k, varargin{3}, ...
                        varargin{4}, refval, local));

                    % Update counter
                    n = n + 1;

                    % If counter is at an even %, display progress
                    if mod((n-1)/num, 0.01) > 0.005 && ...
                        mod(n/num, 0.01) < 0.005
                        fprintf('%0.1f%%\n', n/num*100);
                    end
                end
            end
        end
    end
end

```

```

        end
    end

    % Otherwise, the data is 2-D
    else

        % Run CPU interp2 function to compute the reference
        % values at the specified target coordinate points
        interp = interp2(refX, refY, single(varargin{1}.data),
...
            tarX + i, tarY + j, '*linear', 0);

        % Update the gamma array by returning the minimum
        % of the existing value or the new value
        gamma = min(gamma, GammaEquation(interp, ...
            varargin{2}.data, i, j, k, varargin{3}, ...
            varargin{4}, refval, local));
    end
end

% Otherwise, the data is 1-D
else

    % Run CPU interp function to compute the reference values at
    % the specified target coordinate points
    interp = interp1(refX, single(varargin{1}.data), tarX + i, ...
        '*linear', 0);

    % Update the gamma array by returning the minimum of the
    % existing value or the new value
    gamma = min(gamma, GammaEquation(interp, varargin{2}.data, ...
        i, j, k, varargin{3}, varargin{4}, ...
        refval, local));
end
end

%% Finish up
% Take square root of result
gamma = sqrt(gamma);

% Log completion
if exist('Event', 'file') == 2
    Event(sprintf(['Gamma calculation completed successfully in ', ...
        '%0.3f seconds'], toc));
end

% Clear temporary variables
clear refX refY refZ tarX tarY tarZ interp;

%%%%%%%%%%%%%%%%%%%%%%%%%%%%%%%%%%%%%%%%%%%%%%%%%%%%%%%%%%%%%%%%%%%%%%%%%%%%%%
function gamma = GammaEquation(ref, tar, i, j, k, perc, dta, refval, local)
% GammaEquation is the programmatic form of the Gamma definition as given
% by Low et al in matrix form. This function computes both local and
% global Gamma, and is a subfunction for CalcGamma. Note that this

```



```

% equation returns Gamma-squared instead of Gamma.
%
% The following inputs are used for computation and are required:
%   ref: the reference 3D array. Must be the same size as tar
%   tar: the target 3D array. Must be the same size as ref
%   i: magnitude of x position offset of tar to ref, relative to dta
%   j: magnitude of y position offset of tar to ref, relative to dta
%   k: magnitude of z position offset of tar to ref, relative to dta
%   perc: the percent Gamma criterion, given in % (i.e. 3 for 3%)
%   dta: the distance to agreement Gamma criterion, unitless but relative
%       to i, j, and k
%   refval: if global, the reference value to base the % criterion from
%   local: boolean, indicates whether to perform a local (1) or global (0)
%         Gamma computation
%
% The following variables are returned:
%   gamma: a 3D array of the same dimensions as ref and interp of the
%         computed gamma-squared value for each voxel based on interp and
%         i, j, k

% If local is set to 1, perform a local Gamma computation
if local == 1

    % Gamma is defined as the sqrt((abs difference/relative tolerance)^2 +
    % sum((voxel offset/dta)^2)). The sqrt is removed for computational
    % efficiency.
    gamma = ((tar - ref) ./ (ref * perc / 100)).^2 + ...
            (i/dta)^2 + (j/dta)^2 + (k/dta)^2;
else

    % Gamma is defined as the sqrt((abs difference/absolute tolerance)^2 +
    % sum((voxel offset/dta)^2)). The sqrt is removed for computational
    % efficiency.
    gamma = ((tar - ref) ./ (refval * perc / 100)).^2 + ...
            (i/dta)^2 + (j/dta)^2 + (k/dta)^2;
end

```

REFERENCES

1. Khan, F.M. and J.P. Gibbons, *Khan's the Physics of Radiation Therapy*. 2014: Lippincott Williams & Wilkins.
2. Buckey, C., et al., *Evaluation of a commercially-available block for spatially fractionated radiation therapy*. *Journal of Applied Clinical Medical Physics*, 2010. **11**(3).
3. Zwicker, R.D., A. Meigooni, and M. Mohiuddin, *Therapeutic advantage of grid irradiation for large single fractions*. *International Journal of Radiation Oncology* Biology* Physics*, 2004. **58**(4): p. 1309-1315.
4. Asur, R., et al., *High dose bystander effects in spatially fractionated radiation therapy*. *Cancer letters*, 2015. **356**(1): p. 52-57.
5. Zhang, H., E.L. Johnson, and R.D. Zwicker, *Dosimetric validation of the MCNPX Monte Carlo simulation for radiobiologic studies of megavoltage grid radiotherapy*. *International Journal of Radiation Oncology* Biology* Physics*, 2006. **66**(5): p. 1576-1583.
6. Paganetti, H., *Relative biological effectiveness (RBE) values for proton beam therapy. Variations as a function of biological endpoint, dose, and linear energy transfer*. *Physics in medicine and biology*, 2014. **59**(22): p. R419.
7. Schreuder, N. *Proton Radiation Therapy Technology and Clinical Indications*. [Web] 2015 [cited 2016 20 January]; Available from: <http://web.ornl.gov/sci/aiche/presentations/ProtonTherapy-March-12-2015.pdf>.
8. Cherry, S.R., *Physics in Nuclear Medicine*. 4 ed. 2012: Saunders. 544.
9. *Proton Beam Therapy: Scattering Versus Scanning Treatment Techniques*. [Web] 2011 [cited 2016 21 January]; Available from: https://www.varian.com/sites/default/files/resource_attachments/ProtonTherapy_Scattering%20vs%20Scanning.pdf.
10. Paganetti, H. and T. Bortfeld, *Proton beam radiotherapy-the state of the art*. in: *New Technologies in Radiation Oncology (Medical Radiology Series)*,(Eds.) W. Schlegel, T. Bortfeld and A.-L. Grosu, Springer Verlag, Heidelberg, ISBN, 2005: p. 3-540.
11. Marchand, B., et al. *IBA proton Pencil Beam Scanning: an innovative solution for cancer treatment*. in *Proceedings of EPAC*. 2000.
12. Mohiuddin, M., et al., *High-dose spatially-fractionated radiation (GRID): a new paradigm in the management of advanced cancers*. *International Journal of Radiation Oncology* Biology* Physics*, 1999. **45**(3): p. 721-727.

13. Shultis, J.K. and R.E. Faw, *An MCNP primer*. Kansas State University, Manhattan, 2011.
14. Gooley, J., et al., *MCNP6 User's Manual*, ed. D. Pelowitz. 2012, Los Alamos, NM: Los Alamos National Laboratory.
15. *RayStation Dose Calculation Algorithms*. 2015, RaySearch Laboratories: Stockholm, Sweden.
16. Mackin, D., et al., *Spot-scanning proton therapy patient-specific quality assurance: Results from 309 treatment plans*. International Journal of Particle Therapy, 2014. **1**(3): p. 711-720.
17. Meigooni, A.S., et al., *Dosimetric characteristics of a newly designed grid block for megavoltage photon radiation and its therapeutic advantage using a linear quadratic model*. Medical physics, 2006. **33**(9): p. 3165-3173.